EurJIC
European Journal of Inorganic Chemistry

Minireviews
doi.org/10.1002/ejic.202100367

Chemistry Europe
European Chemical Societies Publishing

Check for updates

VIP *Very Important Paper*

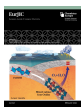

Preparation of Cobalt Nanoparticles

Aliya F. Khusnuriyalova,*[a, b] Maria Caporali,*[c] Evamarie Hey-Hawkins,*[d] Oleg G. Sinyashin,[b] and Dmitry G. Yakhvarov*[a, b]

Dedicated to Prof. Maurizio Peruzzini on the occasion of his 65th birthday

The development of modern chemistry is currently proceeding in several priority areas including investigations focused on the synthesis, stabilisation, and application of transition metal nanoparticles (NPs), which are widely used in physical, chemical, engineering, and biomedical processes. A special place among known transition metal NPs is occupied by cobalt nanoparticles, since they are used for highly important targets, such as creation of new catalysts, magnetic devices, composites, or carriers for drug delivery. The selective preparation of NPs is a difficult task that requires special conditions and has some limitations. In this minireview, we summarise the most successful and most efficient methods for obtaining Co NPs, including chemical and physical aspects of their preparation.

1. Introduction

Nanochemistry is one of the most actively developed areas of modern science, which attracts increasing attention of researchers coming from different fields such as chemistry, physics, biology, catalysis, and medicine.[1–5] The discovery of the peculiar properties of NPs, i.e. objects that have less than 100 nm in at least one dimension,[6] is an important step in achieving miniaturisation in various scientific fields.[7–11]

In particular, metal NPs have been known as colloidal metals for a long time: the first example is colloidal gold discovered by Faraday already in 1857 and named ruby gold for its colour.[12] This ground-breaking discovery represents the birth of what is now called "nanoscience". Examples of applications of metal NPs include metal catalysts,[13,14] magnetic fluids,[15] heat-resistant pigments for glasses[16] and many more. The main areas of application of metal NPs are connected to their peculiar physicochemical properties which are completely different from the bulk material, such as the high surface area to volume ratio (important for instance in catalysis), the surface plasmon excitation (useful in optics) and the interaction at the interface (applications in lubricants, coatings and so on). The wide interest for nanomaterials in various fields of science and industry is connected to the possibility of modifying the properties of bulk materials during the transition to the nanocrystalline state. The famous scientist Feynman said "As we go down in size, there are a number of interesting problems that arise";[17] nanotechnology is meant to face these problems and to create new nanomaterials from the corresponding bulk matter.[18–26] Future scientific and technological progress is characterised by an increase in the possibilities of manipulating matter at ultra-small scales, within the limits of nanometre range.[27]

A plethora of different methods have been investigated for the selective preparation of various nanostructured compounds and materials with desirable properties.[28–30] These methods can be of various nature, such as physical, chemical, electrochemical, biochemical and others. In recent years, there has been a significant increase in the number of publications devoted to the synthesis of transition metal NPs, in particular Co NPs. This is due to the advent of new physical methods, which allow to obtain previously unavailable information, as well as the search for new areas of application of these nano-objects in electronics, optics, surface engineering, chemistry and medicine. In our minireview, we summarise the methods for obtaining cobalt nanoparticles including relevant chemical and physical aspects, and the most important of them are mentioned in Table 1.

2. Transition metal nanoparticles

Nanoclusters, composites, and materials based on transition metal NPs are obtained with a wide range of practically useful

[a] *Dr. A. F. Khusnuriyalova, Prof. Dr. D. G. Yakhvarov*
Alexander Butlerov Institute of Chemistry
Kazan Federal University
Kremlyovskaya 18, 420008 Kazan, Russian Federation
E-mail: khusnuriyalova@gmail.com
yakhvar@iopc.ru
https://www.yakhvarov.com
[b] *Dr. A. F. Khusnuriyalova, Prof. Dr. O. G. Sinyashin, Prof. Dr. D. G. Yakhvarov*
Arbuzov Institute of Organic and Physical Chemistry
FRC Kazan Scientific Center, Russian Academy of Sciences
Arbuzov Street 8, 420088 Kazan, Russian Federation
[c] *Dr. M. Caporali*
Institute of Chemistry of Organometallic Compounds (ICCOM)
Via Madonna del Piano 10, 50019 Sesto Fiorentino, Italy
E-mail: maria.caporali@iccom.cnr.it
[d] *Prof. Dr. E. Hey-Hawkins*
Faculty of Chemistry and Mineralogy
Institute of Inorganic Chemistry
Leipzig University
Johannisallee 29, 04103 Leipzig, Germany
E-mail: hey@uni-leipzig.de

© 2021 The Authors. European Journal of Inorganic Chemistry published by Wiley-VCH GmbH. This is an open access article under the terms of the Creative Commons Attribution Non-Commercial NoDerivs License, which permits use and distribution in any medium, provided the original work is properly cited, the use is non-commercial and no modifications or adaptations are made.

© 2021 The Authors. European Journal of Inorganic Chemistry published by Wiley-VCH GmbH

properties.[31–48] From the viewpoint of creation of new technologies, transition metal NPs occupy a special place among other nanosized particles. They are of great interest due to their peculiar catalytic,[49–57] magnetic,[58–64] mechanical,[65–67] optical,[68–71] electronic,[72–74] and biological[75–79] properties. Most of these applications require chemically stable, well-dispersed, and uniform-sized particles, hence the rapid development of methods for the synthesis of metal NPs.[80–85] In particular, NPs of 3d metals have found application in engineering, chemical and petrochemical industries, aviation, and space technology.[86–92] The research in this field is associated with the discovery of very interesting and practically useful chemical and physical properties of iron, cobalt, and nickel NPs.[93–98] The uniqueness of these metal NPs is primarily related to their magnetic properties,[99–105] which are influenced by many factors, such as chemical composition, type of crystal lattice and its defects, size and shape of the particles, morphology, interaction with the ambient matrix and neighbouring particles.[106–108] Thus, the magnetic properties can be controlled by changing the size, shape, composition and structure of the NPs.[109–111] Currently, magnetic metal NPs are used for microelectronics,[112–114] optical devices and sensors,[115–117] recording and storing information systems,[118,119] and magnetic cooling systems.[120] Additionally, thanks to their biocompatibility, their response to an external magnetic field, and their size, which is comparable to that of biomolecules, magnetic NPs are suitable for theranostic applications. Thus, they can serve both for diagnostics (for instance in magnetic resonance imaging as contrast enhancement) and therapeutics, as magnetically controlled delivery of anticancer drugs and in hyperthermia treatment for localised cancers.[121] It is worth noting the importance of using metal NPs in catalysis. Thus, transition metal NPs are widely used to produce catalysts with almost 100% selectivity, extremely high activity, low energy consumption, and long lifetime. Increased selectivity and activity of the catalysts based on NPs are achieved by controlling the pore size

Aliya Khusnuriyalova was born in Chishmy (Russian Federation) in 1993. She graduated from Alexander Butlerov Institute of Chemistry of Kazan Federal University in 2016. She completed her PhD on the generation of cobalt and nickel nanoparticles under electrochemical reduction's conditions under the supervision of Prof. Dr. Dmitry Yakhvarov in 2021. She is currently working as postdoctoral researcher in the Laboratory "Homogeneous catalysis" of Kazan Federal University. Her main research activity regards the development of new synthetic protocols for the preparation of transition metal nanoparticles and organometallic compounds by electrochemical methods and their application in the fields of homogeneous catalysis.

Maria Caporali got her PhD in Chemistry in 2003 at the University of Florence and soon after she moved to the Technical University of Eindhoven (NL) for a post-doctoral grant. In 2006 she joined CNR ICCOM working on the activation and functionalization of white phosphorus mediated by late transition metals. Her current scientific interests are centred on phosphorus chemistry, catalysis and materials science, ranging from the sustainable conversion of white phosphorus into organophosphorus derivatives to the surface functionalization of 2D black phosphorene with transition metal complexes and nanoparticles and their application in heterogeneous catalysis.

Evamarie Hey-Hawkins has been Professor of Inorganic Chemistry at Leipzig University, Germany, since 1993. She received her diploma (1982) and doctoral degree (1983) at Philipps University Marburg, Germany. After stays in the UK (1984/85) and Australia (1985/87), she completed her habilitation in Marburg (1988). Her scientific interests are organophosphorus chemistry, biologically active boron compounds, and heterometallic transition metal complexes with applications in catalysis and materials science. She has published over 535 papers, edited a book on Smart Inorganic Polymers (with Muriel Hissler), is a member of the European Academy of Sciences, and has received several prestigious awards.

Oleg Sinyashin graduated from Kazan State University (KSU) in 1978. He received his PhD degree from KSU in 1981 and Dr. Sci. degree in chemistry in 1990. He is currently the full member of the Russian Academy of Sciences, and the Director of FRC "Kazan Scientific Center of RAS". His research interests cover chemistry of organophosphorus compounds, synthesis, structure and properties of organometallic compounds, chemistry of fullerenes, electro synthesis of organic and organoelement compounds.

Dmitry Yakhvarov was born in 1974 in Kazan, Russian Federation. He graduated the Department of Physical Chemistry of Kazan State University in 1996. He got his Ph.D. (Candidate of Sciences) in February 2000 and became a Dr. habil. (Doctor of Sciences) in 2012. Since 1995 he is a Chief Scientist at the Arbuzov Institute of Organic and Physical Chemistry of the Federal Research Center "Kazan Scientific Center of Russian Academy of Sciences" and Alexander Butlerov Institute of Chemistry of Kazan Federal University. In 2016 he was awarded an honorary title of "Professor of the Russian Academy of Sciences".

© 2021 The Authors. European Journal of Inorganic Chemistry published by Wiley-VCH GmbH

Table 1. Summary of the main methods for preparation of cobalt nanoparticles.

Method	Size observed	Starting materials	Conditions	Remarks	Ref.
Physical methods					
γ-Radiolysis	5–6 nm	$CoSO_4$, Al_2O_3	γ-Radiolysis: ^{60}Co source at dose rate of 20 Gy min^{-1}, T = 100 °C, 2 h	Co NPs showed superparamagnetic behaviour at room temperature because of their small size and underwent ferromagnetic ordering at lower temperatures −268 °C.	[186]
Femtosecond laser ablation and fragmentation	11–30 nm	Pure disk bulk target of Co (99.9% pure, 4 mm), *n*-hexane, diethyl ether, toluene, 2-propanol, acetone, methanol	Femtosecond laser, processing time of 4 or 60 min	Co NPs growth without using surfactants occurs from light absorption by the colloids through diffusion coalescence and can be controlled by the solvent polarity, the processing time, and the laser power.	[187]
Pulsed laser irradiation	4 nm	$Co_2(CO)_8$, OA, TOPO, 1,2-dichlorobenzene	Q-switched Nd:YAG laser: pulses with a width of 5 ns at a repetition rate of 10 Hz and a wavelength of either 355 or 266 nm, 30 min	The size and the size distribution of the Co NPs could be controlled by adjusting certain reaction conditions, such as the ligand concentration and the wavelength of light.	[188]
Laser irradiation	5 nm	(100) oriented *p*-type silicon wafers, SiO_2, thin Co layer	Laser power of 0.05 W and two scan numbers	A clear hysteresis in the capacitance–voltage (C–V) curve was observed due to the charging effect in the Co NPs in the C–V curve. According to this property, Co NPs in gate oxide can be used in the development of non-volatile memory devices.	[189]
Magnetron sputtering	15–60 nm	*p*-type Si (001) substrates, Co target (99.95% purity)	Direct current power at 50 W, room temperature	NPs can be obtained from magnetron sputtering under positive bias conditions, where both temperature rise and electron charging effects efficiently limit the NPs growth and make the nanoparticle array more uniform.	[193]
Plasma discharge and ultrasonic treatment	4–70 nm	Cobalt plate (size 10 × 15 × 3 mm, purity 99.93%), cobalt electrode tips (length 7 mm, purity 99.8%), ethanol	Electric plasma discharge, ultrasonication, T = 460–600 °C.	The size of Co NPs was dependent on the annealing temperature, in particular their size range increased due to sintering from 4 to 50 nm in the *hcp* crystal structure of α-Co, and from 5 to 70 nm in the *fcc* crystal structure of β-Co after annealing at 460–600 °C.	[194]
Electrospinning and annealing	20 nm	Polyacrylonitrile, cobalt(II) acetylacetonate, DMF, NaOH, $NH_3 \cdot H_2O$, ethanol, ethyl orthosilicate	Electrospinning conditions: positive high pressure of 15 kV, negative high pressure of −3 kV, receiving distance of 18 cm, feed rate of 0.08 mL min^{-1}	Co/N-CNFs with solid and macroporous structures showed excellent ferromagnetic properties at room temperature.	[195]
Thermal decomposition					
Decomposition in the presence of a reactive gas (H_2 or CO)	1.6 nm	[Co(COE)(COD)], PVP, THF	T = 0, 20, and 60 °C, H_2 or CO (300000 Pa)	Co NPs showed superparamagnetic behaviour, and the magnetic moment per atom appeared to be significantly larger than the value known for bulk cobalt due to magnetic surface effect.	[174]
Gravitation differential fast-drying and thermal decomposition under an applied magnetic field	5–20 nm	$Co_2(CO)_8$, toluene, *n*-hexane, Na(AOT)	Externally ultrasonically dispersing, T = 120 °C, 5 h	The self-assembly of prepared Co NPs results in a transition from superparamagnetic cobalt NPs to a ferromagnetic whisker structure.	[196]
Pressure drop-induced decomposition	6–140 nm	$Co_2(CO)_8$, *n*-dodecane, OA, trioctylamine	T = 170 °C, CO pressure: 1.3, 2.3, 3.2, 4.5, and 5.5 bar	The variation of the CO pressure provides a means not only for fine-tuning the size but also to study how the supersaturation affects nucleation rates.	[197]
Rapid pyrolysis in inert atmosphere	3–17 nm	$Co_2(CO)_8$, anhydrous *o*-dichlorobenzene, OA, TOPO, *n*-hexyl phosphonic acid	T = 181 °C	Co NPs arrange in hexagonal arrays on slow evaporation of solvent from a concentrated solution and are stable in air over months.	[198–200]

© 2021 The Authors. European Journal of Inorganic Chemistry published by Wiley-VCH GmbH

Table 1. continued

Method	Size observed	Starting materials	Conditions	Remarks	Ref.
High-temperature thermal decomposition	6–8 nm	$Co_2(CO)_8$, TPP, OA, dichlorobenzene, *n*-heptane, ethanol	T = 200–220 °C, centrifugation	Annealing the NPs at 500 °C under Ar + H_2(5 %) for 3 hours converts the particles from ε-Co to *fcc*-Co. The magnetic properties of the ε-Co NPs depend on the size.	[201]
Post-reductive annealing process	10 ± 1 nm	$Co_2(CO)_8$, 1,2,3,4-tetrahydronaphthalene, OA, dioctylamine, Ketjen carbon	T = 600 °C, Ar + H_2(5 %), 1 h	Co NPs are active and durable for OER due to electron conductivity of the metallic core. The catalyst based on Co NPs assembled into a monolayer array on the working electrode exhibited 15 times higher TOF and mass activity than the Co NPs deposited on conventional carbon black.	[202]
In situ thermal decomposition in ILs	53 ± 22 nm and 79 ± 17 nm	$Co_2(CO)_8$, [DMI][FAP], [DMI][NTf_2], *n*-hexane	T = 150 °C, stirring 250 rpm	The diameter of the Co NPs is 53 ± 22 nm and 79 ± 17 nm for the samples prepared in [DMI][FAP] and [DMI][NTf_2], respectively, by TEM analysis. IL forms a protective layer around the metal NPs and prevents its oxidation, as was confirmed by XRD analysis.	[205]
Decomposition in imidazolium-based ILs	5–8 nm	$Co_2(CO)_8$, [BMI][NTf_2], [DMI][BF_4], [TDMI][NTf_2], *n*-hexane	T = 150 °C, 20–40 min	The size of the Co NPs was controlled by the choice of counter anion of the IL: Co NPs with size of 4.5 ± 0.6 nm and 7.7 ± 1.2 nm were prepared by decomposition of an organometallic precursor in [DMI][BF_4] and [BMI][NTf_2], respectively.	[206]
"Hot injection" method	3–10 nm	$Co_2(CO)_8$, *o*-dichlorobenzene, OA	T = 168–182 °C	The formation of Co NPs was controlled by the temperature of the hot OA solution into which the Co precursor was injected.	[207]
Decomposition under H_2 in imidazolium-based ILs	< 5 nm	[Co(COE)(COD)], [BMI][NTf_2], [TDMI][NTf_2]	T = 100 °C, H_2 (300000–400000 Pa), 4 h	The synthesised Co NPs adopt the non-compact and metastable structure of ε-Co that converts to stable *hcp*-Co at room temperature. [BMI][NTf_2] is a more efficient stabiliser of the NPs.	[208]
Melt infiltration process and thermal treatment	15 nm	$Co(NO_3)_2 \cdot 6H_2O$, γ-alumina powder	T = 450 °C in a hydrogen flow	The catalyst based on Co NPs showed CO conversions up to 76 % with high hydrocarbon productivity and good stability in Fischer-Tropsch synthesis.	[210]
Thermal decomposition	8–200 nm	$Co(OAc)_2 \cdot 4H_2O$, TOP, OAm, OA, 2-pyrrolidinone	T = 260 °C, 90 min, flushing with high-purity N_2 gas	The size of Co NPs was controlled by using various surfactant combinations of TOP, OAm and OA.	[211]
One-pot pyrolysis	6–50 nm	$Co(NO_3)_2 \cdot 6H_2O$, melamine, polyacrylonitrile, DMF	T = 700, 800, and 900 °C	Co NPs prepared at 900 °C have a very high number of active sites; this feature in conjunction with the mesoporous fluffy mCN structure that facilitates a high dispersion of Co NPs contributes to an enhanced catalytic activity in hydrogenation of nitroarenes.	[213]
High temperature treatment with hydrogen	1–8 nm	SWCNT, cobalt(II) acetylacetonate, dichloromethane	T = 300, 400, and 500 °C, ultrasonication	The size and shape of Co NPs were controlled by varying the temperature at which the hydrogen treatment takes place.	[215]
Size-control synthesis inside of hollow carbon spheres	5–44 nm	PS-*b*-PAA, $Co(NO_3)_2$, hydrazine, ethanol, resorcinol, formaldehyde, CTAB	T = 600 °C, 10 °C min^{-1}, 2 h	Concentration of PAA in polymer and composition of the Co NPs (variation between Co, CoO and Co_3O_4) influences the size of Co NPs.	[216]
Thermal decomposition using *N*-doped carbon nanoshells	20 nm	$Co(NO_3)_2 \cdot 6H_2O$, 1,4,7,10-tetraazacyclododecane, dicyandiamide, perchloric acid	T = 700–900 °C, 1 h	The morphology and properties of Co NPs can be regulated by the pyrolysis temperature. Catalyst Co@N-C-800 showed bifunctional catalytic activities for ORR and OER.	[217]

© 2021 The Authors. European Journal of Inorganic Chemistry published by Wiley-VCH GmbH

Table 1. continued

Method	Size observed	Starting materials	Conditions	Remarks	Ref.
Synthesis on porous organic polymers	–	$Co(NO_3)_2 \cdot 6H_2O$, hydrazine, ethylene diamine, cyanuric chloride, 1,4-dioxane	T = 180, 300, and 500 °C	Co NPs were stabilised by the amine groups of the porous organic polymers. Co-EPOP-based electrocatalysts showed effective electrocatalytic activity in water-splitting reactions. For instance, HER activity of the catalysts followed the order Co-EPOP-500 > Co-EPOP-300 > Co-EPOP-HT > Co NPs.	[218]
Hydrothermal and solvothermal syntheses					
One-pot synthesis by combination of hydrothermal and carbonisation reactions	30–75 nm	OMC, $Co(NO_3)_2 \cdot 6H_2O$, formaldehyde, hydrochloric acid	T = 100 °C for 10 h, T = 600 °C for 3 h	The catalyst based on CoNPs@OMC has good cycling stability for the hydrogenation reaction of *p*-nitrophenol and nitrobenzene and also showed good catalytic selectivity for C_5 hydrocarbons in the Fischer-Tropsch synthesis.	[220]
Solvothermal method in supercritical methanol	10–50 nm	$Co(NO_3)_2 \cdot 6H_2O$, supercritical methanol	T = 200–400 °C, 300 bar, 30 s to 15 min	Methanol was used as reaction medium and as reducing agent. The obtained Co NPs showed a ferromagnetic behaviour according to SQUID measurements.	[221]
Reductive supercritical hydrothermal process	no information	$Co(OAc)_2 \cdot 4H_2O$, methanol, formic acid	T = 340–420 °C, 221 bar	Co NPs were highly crystalline and exhibited little surface oxidation. The synthesis of NPs proceeded via two tandem reactions, the formation and follow-up reduction of cobalt monoxide.	[222]
Reduction by borohydride on RGO sheets in aqueous medium	6–123 nm	$CoCl_2 \cdot 6H_2O$, $NaBH_4$, graphite powder,	Room temperature, T = 90 °C, 0.6 T magnetic field	The cube-shaped Co-RGO (10 nm) were prepared by the hydrothermal method at non-equilibrium conditions at 90 °C, spherical Co-RGO (6 nm) by the co-precipitation method at room temperature, and rod-like Co-RGO (123 nm length, 6 nm width) by an applied magnetic field with co-precipitation. All syntheses were carried out without any surfactant or capping agent.	[223]
Reduction of cobalt salts					
Reduction with borohydride	2–11 nm	$CoCl_2$, $LiBEt_3H$, dioctylether, THF, OA, TOP	Room temperature, T = 100 and 200 °C	The growth and steric stabilisation of the Co NPs were controlled by the combination of OA and TOP. The ε-Co structure was transformed to the *hcp* structure by annealing the NPs at 300 °C.	[227]
Reduction in the presence of $NH_3 \cdot H_2O$ and DMF	6 nm	$CoCl_2 \cdot 6H_2O$, $NH_3 \cdot H_2O$, DMF	T = 160 °C, 12 h	DMF was used as solvent and reducing agent for producing Co NPs with narrow size distribution.	[229]
Reduction using 1,2-dodecanediol as reducing solvent at high temperature	15–20 nm	$Co(OAc)_2 \cdot 4H_2O$, OA, diphenyl ether, 1,2-dodecanediol	T = 250 °C, 30 min	The strong interaction between OA and Co NPs resulted in a covalent Co–O bond which enhanced the stability of the metal colloid.	[230]
One pot synthesis by OA	7.8–9.2 nm	$CoCl_2 \cdot 6H_2O$, TPP, $NaBH_4$, OA	T = 190 °C	OA acts both as the reducing agent, solvent and surfactant. Co nanospheres or Co nanorods (*hcp*) can be prepared by varying the reaction time.	[231]
Reduction by hydrazine in alkaline medium	30–70 nm	$CoSO_4$, hydrazine, NaOH	T = 70 °C	The size of the Co NPs determined by TEM was 50–70 nm, but XRD analysis by the Scherrer formula gave a size around 24–49 nm.	[233]
Reduction by hydrazine in the presence of citric acid	400 nm	$CoSO_4 \cdot 7H_2O$, hydrazine, citric acid	T = 25 and 80 °C, 1–2 h	Citric acid influenced the reduction reaction and the formation of *hcp* Co NPs predominantly.	[234]

© 2021 The Authors. European Journal of Inorganic Chemistry published by Wiley-VCH GmbH

Table 1. continued

Method	Size observed	Starting materials	Conditions	Remarks	Ref.
Reduction by hydrazine in ethanol/alkaline medium	200–230 nm	$CoCl_2 \cdot 6H_2O$ or $CoSO_4 \cdot 7H_2O$, hydrazine, NaOH, ethanol	Room temperature	The *fcc* and *hcp* phase of Co NPs were obtained. The latter grew more regularly and larger, and the coercivity of the sample increased from 480 to 680 Oe by heating at 200 °C for 2 h.	[235]
Reduction by borohydride on natural polymers	5–10 nm	$CoCl_2$, $NaBH_4$, cellulose filter paper, chitosan	Room temperature, 5 h	The heterogeneous catalyst based on Co NPs was tested in the hydrogenation of 2,6-dinitrophenol. The catalyst proved to be efficient and stable after four consecutive runs.	[236]
Reduction by borohydride on a starch hydrogel	30 nm	$Co(NO_3)_2 \cdot 6H_2O$, $NaBH_4$, starch, citric acid	Room temperature, 30 min	Heterogeneous catalyst based on starch hydrogel-loaded Co NPs showed high catalytic activity in the hydrogen production from hydrolysis of $NaBH_4$ which was maintained over five catalytic runs.	[237]
One pot process by using phthalocyanine macrocycle	3 nm	$CoCl_2$, $NaBH_4$, nitrophthalonitrile, ammonium molybdate, urea, $Na_2S \cdot 9H_2O$, DMSO, *n*-pentanol	T = 40 and 160 °C, 22 h (preparation of cobalt tetraminephthalocyanine), T = 4–10 °C, 30 min	The TAP stabilised and prevented oxidation of Co NPs for a week. This agent was more efficient in the stabilisation of Co NPs in comparison with common capping agents and in preventing the formation of a surface oxide layer.	[238]
Synthesis in colloidal assemblies	5.5–5.8 nm	$CoCl_2$, $NaBH_4$, AOT, TOP, pyridine	Room temperature	The magnetic properties of Co NPs are strongly dependent on the self-organisation of nanocrystals. The collective properties of 2D networks of Co NPs are determined by the dipolar magnetic interaction between adjacent particles.	[239, 240]
Synthesis in micellar system	6–8 nm	$Co(OAc)_2$, lauric acid, $NaBH_4$, Na(AOT)	Room temperature	The reducing agent modified the nucleation and growth processes of formation of Co NPs. The low concentration of $NaBH_4$ and the structural and chemical properties of the micellar system led to production of small size 6–8 nm polydisperse Co NPs.	[241]
Reduction by borohydride in nonaqueous solution	4.7 nm	$CoCl_2$, $NaBH_4$, ethanol, OA	Room temperature	The oxidation and the formation of cobalt borides were minimised by using ethanol as medium in the reduction reaction.	[242]
Reduction by borohydride in tetraglyme	20–100 nm	$CoCl_2$, $NaBH_4$, tetraglyme, OA, OAm, PVP	T = 200–270 °C, Ar + H_2(5%), 30 min	Crystalline *hcp* Co NPs with high saturation magnetisation (143 emu g^{-1}) and with a moderate coercivity of 500 Oe were obtained by this method.	[243]
Reduction with borohydride by deposition on α-Al_2O_3	50 nm	$CoCl_2 \cdot 6H_2O$, $NaBH_4$, γ-Al_2O_3, cyclohexane	T = 500 °C, Ar flux, sonication, T = 1300 °C (to produce α-Al_2O_3 from γ-Al_2O_3)	The nanocatalyst based on Co NPs was applied for the production of hydrogen and gave satisfactory results.	[244]
Reduction in aqueous solution	5–6 nm	$CoCl_2 \cdot 6H_2O$, $NaBH_4$	Room temperature, mechanical stirring, Ar flux	The unsupported Co NPs showed catalytic activity in the HER reaction by producing H_2 with 90% yield at 500 °C.	[246]
Synthesis by two reducing agents	50–70 nm	$CoCl_2 \cdot 6H_2O$, $NaBH_4$, L-AA, MWCNTs (95% of purity), polyvinylidene fluoride	Room temperature	Co NPs without any specific agglomeration on the surface of MWCNTs were prepared by a facile and green method using $NaBH_4$ and L-AA. Catalytic membranes incorporating Co NPs could be used as efficient catalysts for reduction of *p*-nitrophenol to *p*-aminophenol.	[247]

© 2021 The Authors. European Journal of Inorganic Chemistry published by Wiley-VCH GmbH

Table 1. continued

Method	Size observed	Starting materials	Conditions	Remarks	Ref.
Thermal decomposition (i), polyol process (ii), reduction of cobalt salt by borohydride (iii)	3–8 nm	(i) $Co_2(CO)_8$, 1,2-dichlorobenzene, TOPO, OA; (ii) $Co(OAc)_2$, 1,2-dodecanediol, diphenyl ether, OA; (iii) $Co(OAc)_2$, $NaBH_4$, OA, ethanol	(i) T = 180 °C, centrifugation; (ii) T = 250 °C, 30 min, centrifugation; (iii) Room temperature, centrifugation	Co NPs with 6–8 nm size were prepared by thermal decomposition (i). In the polyol process (ii), working at high temperatures, undefined-shape Co NPs were formed. In the reduction method (iii) with $NaBH_4$, the reducing agent has a key role in the size distribution of the Co NPs.	[248]
The polyol process					
Reducing the metal ions in polyol	50–200 nm	$Co(OAc)_2 \cdot 4H_2O$, $CoCl_2 \cdot 6H_2O$, EG or trimethylene glycol, NaOH	Room temperature, T = 180–200 °C	Accelerating the oxidation reaction of EG enhanced the reaction due to presence of OH^- ions. The reduced form cobalt alkoxide or cobalt hydroxide plays a decisive role in determining the physical properties of the Co NPs.	[254]
Microwave polyol process	40 and 81 nm	$Co(OAc)_2 \cdot 4H_2O$, OA, NaOH, $PdCl_2$, polyacrylic acid, PVP, ethanol	T = 165–185 °C, microwave power at 800 W, 240 s	The saturation magnetisation was 39.1 and 29.5 emu g^{-1} for Co NPs with a size of 40 and 81 nm, respectively, because the total magnetic moment per atom is enhanced with decreasing particle size.	[256]
Polyol process using a hydrazine complex	35–200 nm	$Co(OAc)_2$, EG, hydrazine, PVP	T = 185–190 °C, 30 min	Co NPs with an average size of 35 nm showed the highest coercivity (109 Oe). The size of NPs was controlled by varying the concentration of PVP.	[257]
Size-controlled synthesis	1.8–2.8 nm	$CoCl_2 \cdot 6H_2O$, EG, PVP, $NaBH_4$	T = 7–100 °C, 1 h, intensive magnetic stirring	The size of Co NPs depended on the temperature and increased with the increase of reduction temperature.	[259]
Facile low-temperature synthesis	2–7 nm	$CoCl_2 \cdot 6H_2O$, EG, N_2H_4, NaOH	T = 80 °C, 1 h, stirring 420 rpm	EG was used as both solvent and protective agent.	[253]
Polyol process using long-chain carboxylates	18–38 nm	$Co(OAc)_2 \cdot 4H_2O$, 1,2-butanediol, $RuCl_3 \cdot xH_2O$, NaOH micro-pearls, dodecanoic acid	T = 175 °C, stirring 0–400 rpm	The stirring rate has a significant impact on the shape and size of Co NPs. The intensity of mechanical agitation has a remarkable effect on morphology and influenced the structure and magnetic properties of Co NPs.	[260]
One-step seed-mediated synthesis	15–50 nm	$Co(OAc)_2 \cdot 4H_2O$, $RuCl_3 \cdot xH_2O$, $IrCl_3 \cdot xH_2O$, NaOH, 1,2-butanediol or 1,2-propanediol, dodecanoic acid, palmitic acid	T = 175 or 215 °C, 10–30 min	Co NPs showed different shapes such as rods, platelets and hourglass-like particles which could be tuned by varying the seed ($RuCl_3$, $IrCl_3$) structures.	[261]
Synthesis in aqueous media and EG system	2–75 nm	$CoCl_2 \cdot 6H_2O$, H_2O, EG, CTAB, $NaBH_4$, hydrazine, sodium citrate, OA	Room temperature, T = 197 °C	The reduction by $NaBH_4$ led to the formation of quasi-monodispersed Co NPs of size 2 nm but with some impurities. In the presence of hydrazine (mild reducer), Co NPs have larger size and are organised in spherical microagglomerates.	[262]
Electrochemical methods					
Electrochemical synthesis	2–10 nm	Co anode (sacrificial electrode), two Pt cathodes, Pt pseudo-reference electrode, $(n\text{-Oct})_4NBr$, THF, acetonitrile	DC, current density 1 mA cm^{-2}, room temperature	Co NPs were prepared by the process based on anode oxidation with migration of the generated cations to the cathode, which reduced them to the zero oxidation state and formed metallic atoms adsorbed on the surface and stabilised by capping agent (electrolyte).	[269]
Electrochemical synthesis	2–5 nm	Co anode (2 cm × 5 cm × 1 mm), Pt cathode (2 cm × 5 cm × 1 mm), tetrabutylammonium nitrate, acetonitrile, OA, TPP	DC, current density 1–5 mA cm^{-2}, T = 20 °C, 90 min	The size of Co NPs was controlled by variation of the current density. Co NPs were protected by a combination of surfactants such as OA and the ligand TPP, which strongly interact with Co surface atoms.	[270]

© 2021 The Authors. European Journal of Inorganic Chemistry published by Wiley-VCH GmbH

Table 1. continued

Method	Size observed	Starting materials	Conditions	Remarks	Ref.
Electrodeposition onto aluminium foils	30–70 nm	Pt wire (counter electrode), Ag/AgCl (reference electrode), Al foils 0.5 cm^2 area (working electrode), $CoSO_4 \cdot 7H_2O$, $NaSO_4$, H_3BO_3	DC, potential range from −1.0 V and −1.35 V, T = 25 ± 0.01 °C	An effect of amount of electric charge on the size of Co NPs was observed. An increase in the mean size of Co NPs occurred when the amount of the electric charge was changed from 10.60 to 52.3 mC.	[271–274]
Mediated electrosynthesis	5–30 nm	$Co(BF_4)_2 \cdot 6H_2O$, anthracene, Bu_4NBF_4, Bu_4NCl, DMF, cobalt plate 4.2 cm^2	DC 25 mA, potential −2.3 V, room temperature	Co NPs were synthesised by using anthracene as a mediator in the electrolysis at the potential of anthracene reduction to the radical anion in aprotic DMF and generating $[CoCl_4]^{2-}$ ions by dissolving the bulk cobalt anode.	[275]
Electrochemical reduction	9–10 nm in diameter and 30–32 nm in length	$CoBr_2$, bpy, DMF, cobalt anode (3.0 cm, d = 1.0 mm)	DC 16 mA, room temperature, 30 min	Superparamagnetic cylindrical Co NPs were prepared due to the disproportionation reaction of the electrochemically generated cobalt(I) mononuclear complexes.	[276]

and the characteristics of the used nanoparticles.[122] All these aspects explain the great interest of specialists belonging to different fields towards transition metal NPs.[123–125]

3. Properties of cobalt nanoparticles

Co NPs have received special interest among 3d metals. Cobalt is widely and diversely used in various chemical areas,[126] biology[127] and medicine,[128] which are associated with the remarkable properties of this metal, its alloys and salts. It is noteworthy that cobalt has been used in the production of various industrially important alloys,[129] batteries,[130,131] pigments, and colours. Thus, cobalt is used widely as one of the metals needed to create hard permanent magnets with high coercivity, such as the aluminium-nickel-cobalt (Al–Ni–Co, "Alnico") alloy series. Alnico magnets are used in motors, hard disk drives, and sensors.[132–135] Magnetic resonance imaging (MRI) is another example of an application for these magnetic alloys.[136,137] Presently CoNPs are the most important and very efficient NPs in catalysis. Powdered cobalt, its oxides, salts and complexes have found application either as homogeneous or heterogeneous catalysts in fundamental chemical processes (for instance hydroformylation of olefins, Fischer-Tropsch reaction) and in petrochemical industry (hydrodesulfurisation of oil).[138–153] Another important application is related to the use of the artificially obtained radioactive isotope ^{60}Co as a source for generation of high energy gamma rays to perform the radiolysis of water in the radiolytic syntheses of transition metal NPs on supports.[154] This approach has the advantage to be clean, since it avoids the formation of by-products and has refined control on shape and size of NPs. Additionally, ^{60}Co is used for sterilisation of medical equipment[155] and radiography.[156] From the viewpoint of biological function, cobalt plays an important role as the metal centre in vitamin B_{12}. This notwithstanding, excessive exposure causes a variety of adverse health effects.[157] Therefore, it is important to monitor the concentration of cobalt in various forms in the human body, atmosphere, soil, etc. However, this does not diminish high interest towards cobalt due to its unique properties and many applications.

However, it is worth noting that the remarkable properties of cobalt have become even more interesting by the discovery of unusual physical and chemical properties of Co NPs, associated with the presence of the so-called "quantum size effects". These effects are caused by the fact that the density of states in the valence band and in the conduction band changes markedly with a decrease in size and the transition from a macroscopic body to the scales of several hundred or several thousand atoms. It affects the electrons, and thus primarily magnetic and electric properties. The "continuous" density of states, typical of matter in the bulk, is replaced by discrete levels which depend on the particles' size and on the distances between them.[158] Another important property affecting the physical and chemical properties of NPs as their size decreases is the increase of the relative share of "surface" atoms under different conditions (coordination number, symmetry of the local environment and others). A serious change in the properties of "surface" atoms occurs and as a consequence, the interaction between atoms located on the surface and atoms inside the particle also changes, which can lead to a fundamental change in physical properties.[159] For instance, cobalt nanoclusters have shown an enhancement of magnetisation compared to bulk cobalt due to the enhanced magnetisation of surface atoms as a result of their small size. Another important point related to the magnetic properties are the allotropic forms of metallic cobalt. There are three well-known allotropes: anisotropic high-coercivity *hcp*-Co (hexagonal close packed), which is the stable phase at room temperature, symmetric low-coercivity *fcc*-Co (face-centred cubic), stable at temperatures above 450 °C, and pseudo-cubic *ε*-Co.[160] In addition, Co NPs with a size up to 20 nm are single-domain particles with quantum size effects, large magnetic anisotropy, quantum tunneling of magnetisation, and superparamagnetism.[161] It should be noted that the metastable phase *ε*-Co displays properties between the *hcp* and *fcc* phases

© 2021 The Authors. European Journal of Inorganic Chemistry published by Wiley-VCH GmbH

which is of high interest for creating functional nanomaterials with useful properties. Co NPs have found applications in biomedicine, as they have an intrinsic advantage in drug delivery and magnetic resonance imaging,[162] thanks to their magnetic properties. Typically, magnetic Co NPs are coated with surfactants (i.e. oleic acid) and polymers (i.e. dextrin, polyethylene glycol) to enhance biocompatibility, provide functionality and prevent agglomeration.[163] Thus, nanoscale Co particles offer a new step in the discovery and deepening of the practically significant properties of this metal.[164]

4. Preparation of cobalt nanoparticles

Many different methods for the synthesis of monodispersed Co NPs have been proposed. This variety can be summarised in physical methods (Section 4.1), chemical methods (Sections 4.2, 4.3, 4.4, and 4.5) and electrochemical methods (Section 4.6).

The chemical methods, which include thermal decomposition, hydrothermal synthesis, and the polyol process, are based on the reduction of the most suitable precursor, usually various inorganic, organic, or organometallic cobalt reagents. These procedures have the advantage to be relatively simple and do not require special equipment, while this is not the case for physical methods. In particular, the reduction of cobalt salts in solution is less expensive and fast, and thus highly desirable for future applications and large-scale production. In most cases, the synthesis of transition metal NPs by simple reduction of metal salt precursors proceeds under environmentally friendly conditions, which constitutes a primary task in the development of safe technologies.

Doing a brief historical survey, the study of nanoscale cobalt particles began in the 1970s. In the first publications, Co NPs were defined as "ultra-dispersed" particles. In 1977, Hayashi and coworkers produced ultrafine particles (UFPs) by gas-evaporation technique. They obtained Co particles in the size range of 20–200 nm.[165] Kajiwara and coworkers[166] prepared ultrafine particles, 20–500 nm in diameter, by a "hydrogen-plasma-metal reaction" method. The UFPs were produced by forced evaporation of a button-shaped mother alloy, which was arc melted with 260 A and 22–25 V in an argon/hydrogen mixture (1:1 by volume) at 0.1 MPa. At the same time, methods for preparing Co NPs by chemical reduction have been developed. Thus, Fievet and coworkers[167] described the polyol process for the preparation of micron and submicron size Co particles. Yiping and coworkers synthesised UFP of cobalt having diameters in the range of 5–120 nm by reduction of metal halide solutions in bis(2-methoxyethyl) ether (diglyme) with lithium metal. Additionally, they observed that the size was dependent on the reaction temperature.[168] Klabunde and coworkers studied the reduction of $CoBr_2$ with $NaBH_4$ in diglyme[169] and in water[170] to obtain monodisperse ultrafine Co particles. A different procedure was followed by Chen and coworkers[171] who used the microemulsion method for the preparation of Co NPs with average diameters of 1.8 to 4.4 nm. Functionalised reverse micelles have been used by Pileni and coworkers to synthesise Co NPs having different size and shape.[172] Becker's group worked extensively with transition metal cluster colloids.[173] They could synthesise cobalt clusters containing about 1000 atoms with a narrow size distribution, via electrochemical reduction of cobalt ions produced in an undivided electrochemical cell by anodic dissolution of a sacrificial cobalt anode.

Since the early 1980s, one of the main targets has been to prepare very small Co NPs with a narrow size distribution. In this regard, Chaudret and coworkers proposed a successful route, by thermal decomposition of an organometallic precursor,[174,175] see Section 4.2.

Recently, other methods for producing Co NPs have been developed,[176,177] for instance mechanosynthesis, which refers to reactions induced by mechanical processes, such as milling or grinding. The advantage of performing reactions directly between solids excludes organic or aqueous solvents, which can lead to side reactions and have to be removed at the end of the process.[178–180] Other techniques involve sonochemical synthesis of Co NPs,[181,182] and the above-mentioned electrochemical synthesis.[183–185]

4.1. Physical methods

A typical feature of physical methods is the production of particles by the so-called "top-down" approach, which is opposite to chemical methods characterised by a "bottom-up" approach, namely production of NPs from single atoms. The physical methods are nowadays widely used for the preparation of metal NPs, and one of the most common methods is laser ablation.

In the 1990s, Kulshreshtha and coworkers[186] prepared nanosized cubic Co particles in three different forms by γ-radiolysis of a $CoSO_4$ solution: as an aqueous sol, as a self-supporting powder and dispersed on the surface of Al_2O_3. The particles of the Co sol exhibited a *fcc* structure with an average crystallite size of 5–6 nm. Interestingly, they showed superparamagnetic behaviour at room temperature because of their small size and underwent ferromagnetic ordering at lower temperatures ($T = -268\,^{\circ}C$).

The synthesis of Co NPs by femtosecond laser ablation and fragmentation was described by Boyer and Meunier (Figure 1).[187] The authors studied the influence of the solvent and other reaction parameters on the synthesis of Co NPs avoiding the use of surfactants. Solvent polarity, processing time and laser power were key parameters for controlling the growth of the NPs.

Thanh and coworkers[188] reported the synthesis of Co NPs with a diameter of 4 nm by using pulsed laser irradiation to decompose dicobalt octacarbonyl $Co_2(CO)_8$ in a solution containing trioctyl-λ^5-phosphanone (TOPO) as stabilising ligand. The size of the NPs could be controlled by varying the ligand concentration and the wavelength of the laser light. Producing Co NPs with such a small size is very appealing for biomedical applications, since this size allows the rapid renal clearance from the body and thus avoids any possible toxic effects of prolonged exposure to Co.

© 2021 The Authors. European Journal of Inorganic Chemistry published by Wiley-VCH GmbH

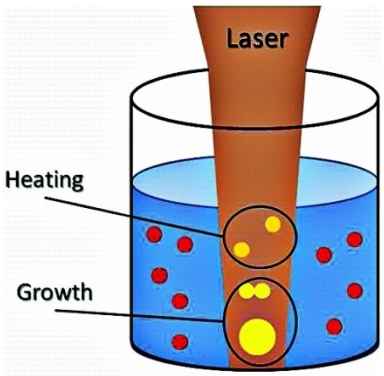

Figure 1. Process for preparation of Co NPs by femtosecond laser ablation and fragmentation. Reproduced from ref. [187], Copyright (2012), with permission from the American Chemical Society.

Co NPs were uniquely fabricated by using a laser irradiation technique by Hong and coworkers.[189] In this way, Co NPs with a narrow size distribution (around 5 nm) were efficiently fabricated and embedded in SiO_2 (Figure 2). Capacitance–voltage (C–V) electrical measurements were conducted on the fabricated device, and a clear hysteresis in the C–V curve was observed due to the charging effect in the Co NPs. Thus, laser irradiation is one of the most efficient processes for formation or insertion of metal NPs into gate oxides, which is relevant for the development of non-volatile memory devices.[190,191]

Besides laser ablation, either using a continuous wave or a pulsed beam laser, another common method to produce NPs is the magnetron sputtering. In this process, a target or a metal precursor is bombarded with a plasma (energetic ions of inert gases, such as argon or helium), and the forceful collision of these energetic ions with the target ejects metal atoms which are then deposited on the substrate material forming a metallic film.[192] In this regard, Chung and Liu demonstrated that high purity Co NPs (99.95 %) ranging from a few to tens of nm in diameter can be easily prepared by direct current (DC) magnetron sputtering on *p*-type Si (001) substrates at room temperature.[193]

An advanced and cost-effective synthesis was successfully realised by Qin and coworkers who developed a protocol for the preparation of Co NPs encapsulated in graphitic shells. The synthesis was carried out by using an electric plasma discharge generated in an ultrasonic cavitation field of liquid ethanol, followed by separation, drying and annealing of NPs in a tube furnace at 460 or 600 °C. The size of Co NPs was dependent on annealing, in particular their size range increased due to sintering from 4 to 50 nm in the *hcp* crystal structure of α-Co, and from 5 to 70 nm in the *fcc* crystal structure of β-Co after annealing at 460 or 600 °C correspondingly (Figure 3).[194]

The groups of Sun, Liao and Zhang carried out *in situ* preparation of Co NPs deposited in *N*-doped carbon nanofibres (Co/N-CNFs) by electrospinning and annealing. In detail, the nanocomposites are synthesised by carbonisation of electrospun polyacrylonitrile/cobalt acetylacetonate nanofibres in an argon atmosphere. The solid Co/N-CNFs have lengths up to dozens of microns with an average diameter of ca. 500 nm and possess abundant Co NPs that have an average size of about 20 nm and are located on both the surface and within the fibres. The phase composition and the crystal structure of Co/N-CNFs were studied by X-ray diffraction analysis (XRD) and Raman spectroscopy, see Figure 4. The resulting nanomaterial

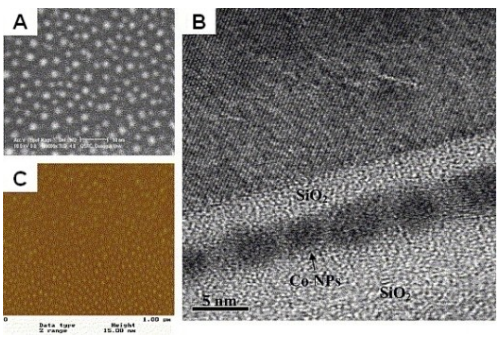

Figure 2. Structural images of Co NPs measured by scanning electron microscopy (SEM) (A), atomic force microscopy (AFM) (B), and transmission electron microscopy (TEM) (C). The TEM image shows a cross-section of the sample consisting of SiO_2 (3 nm)/Co NPs (4.5 nm)/SiO_2 structures on Si substrate (20 nm). Reproduced from ref. [189], Copyright (2007), with permission from Elsevier.

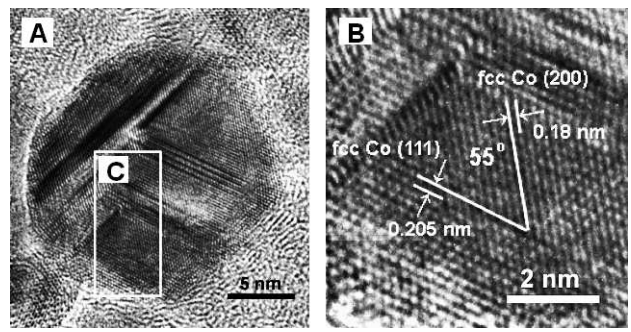

Figure 3. High-resolution transmission electron microscopy (HRTEM) image of an individual *fcc* β-Co nanocrystallite annealed at 460 °C (A) and the enlarged image of the area surrounded by rectangle C (B). Reproduced from ref. [194], Copyright (2007), with permission from Elsevier.

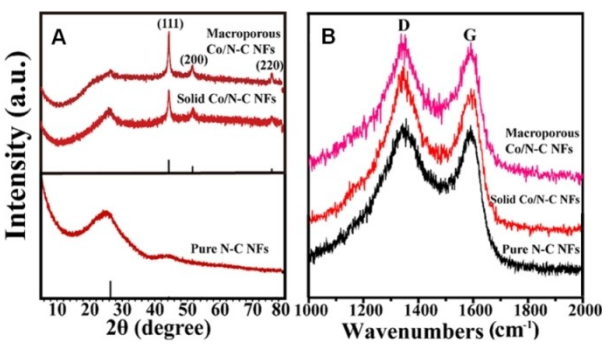

Figure 4. XRD patterns (A) and Raman spectra (B) of macroporous and solid Co/N-CNFs, and pure N-CNFs. Reproduced from ref. [195], Copyright (2018), with permission from the American Chemical Society.

© 2021 The Authors. European Journal of Inorganic Chemistry published by Wiley-VCH GmbH

has shown excellent properties as electromagnetic wave absorber.[195]

However, the structure and spatial arrangement of the NPs obtained by physical methods can vary widely. Moreover, the obtained NPs can maintain the structural properties of the bulk precursor, and this represents one of the main advantages of physical methods. In general, physical methods, adopted for the synthesis of NPs, involve intense heat or force acting on the starting material. This is a key point, and as a direct consequence, the resulting NPs have an increased level of free energy and pure chemical composition.

4.2. Thermal decomposition

One of the main limitations of the physical methods is the formation of NPs with unequal size distribution and crystallinity. In this regard, thermal decomposition, where a suitable metal precursor is decomposed in the presence of organic surfactants, is useful. This process yields improved samples with good size control, narrow size distribution and good crystallinity of individual and dispersible magnetic metal NPs.

One of the pioneering works using the method of thermal decomposition was presented by Chaudret and coworkers.[174] The organometallic precursor [Co(COE)(COD)] (with COE = cyclooctenyl, COD = cycloocta-1,5-diene) reacts with H_2 or CO (300 kPa) in the presence of 1-ethenylpyrrolidin-2-one (PVP) at different temperatures (T = 0, 20 and 60 °C) to give a colloidal solution containing *fcc* Co NPs of the size $\leq$ 1 nm, and about 1.4 and 1.8 nm, respectively. Due to their size, they display superparamagnetic behaviour, and the magnetic moment per atom appeared to be significantly larger than the value known for bulk cobalt, a feature that has been attributed to the magnetic surface effect.

Yin and Wang prepared three different kinds of crystalline Co NPs by thermal decomposition of dicobalt octacarbonyl in toluene.[196] The two-dimensional self-assembly of Co NPs with an average particle size of 9.2 nm (Figure 5) has been achieved by a gravitation differential fast-drying method. Another type was the macroscopic whisker-shaped assembly, formed by Co NPs having 8 nm average size, prepared by thermal decomposition under an externally applied magnetic field. The third sample, a one-dimensional densely packed self-assembly induced by magnetic interaction, was prepared using Co NPs with irregular shape and larger particle sizes. Thus, the formation of these different structures was attributed to the magnetic properties of cobalt particles with different sizes.

The method of thermal decomposition has been investigated also by Johans and coworkers, adding some improvements, as a pressure drop-induced process, in which the supersaturation during the thermal decomposition of $Co_2(CO)_8$ was controlled by a fine regulation of the carbon monoxide pressure.[197] The particle size may vary in a very broad range, i.e. from 6 nm to 130 nm in diameter, by changing accurately the CO pressure between 1.3 and 5.5 bar (Figure 6). Thus, the variation of the CO pressure provides a means not only for fine tuning the size but also to study how the supersaturation affects nucleation rates.

Puntes, Krishnan and Alivisatos produced monodispersed, stabilised, defect-free ε-Co NPs, with spherical shapes and sizes ranging from 3 to 17 nm, where size distribution and shape of the NPs were controlled by varying the surfactants, namely (9*Z*)-octadec-9-enoic acid (OA), phosphonic oxides and acids.[198–200] Carrying out the rapid pyrolysis of dicobalt octacarbonyl in an inert atmosphere, high-quality magnetic colloidal dispersions were produced. Remarkably, they were stable over months, as confirmed by XRD, TEM and related spectroscopies, energy-dispersive X-ray spectroscopy (EDX) and electron energy loss spectroscopy (EELS).

In the research group of Gao, the synthesis of Co NPs by thermal decomposition of dicobalt octacarbonyl in the presence of triphenylphosphane (TPP) and OA was studied.[201] The reason behind the use of TPP and OA was the control of particle growth, their stabilisation towards aggregation and oxidation. An in-depth characterisation by X-ray photoelectron spectroscopy (XPS), XRD and infrared spectroscopy showed that the synthesised Co NPs possess ε-phase crystallinity and that they are stable against air oxidation in hydrocarbon solvent.

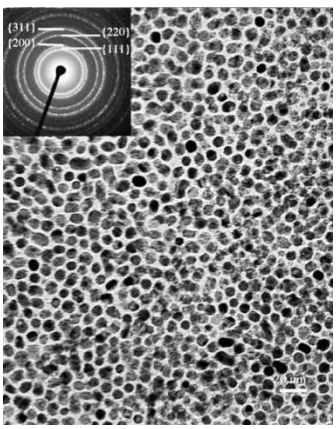

Figure 5. Ordered self-assembly of crystalline Co NPs. The inset is an electron diffraction pattern from the NPs showing the *fcc* structure. Reproduced from ref. [196], Copyright (1999), with permission from Elsevier.

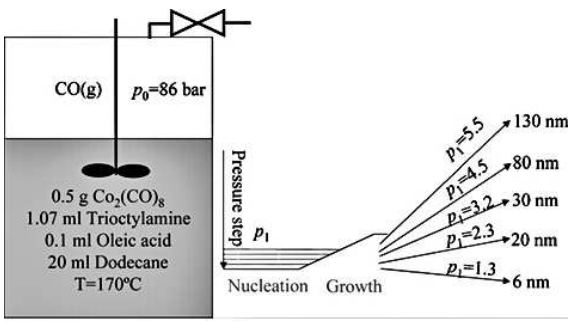

Figure 6. Schematic presentation of the autoclave and reactants for the synthesis of Co NPs via pressure drop-induced decomposition. Reproduced from ref. [197], Copyright (2008), with permission from Elsevier.

© 2021 The Authors. European Journal of Inorganic Chemistry published by Wiley-VCH GmbH

Sun and coworkers described the preparation of highly air-stable Co NPs[202] through a post-reductive annealing process. Co NPs prepared by thermal decomposition of dicobalt octacarbonyl, were deposited on Ketjen carbon (C–Co) through sonication and were then annealed in a flow of argon and 5% H_2 at 600 °C for 1 h. This reductive annealing process reduces the surface cobalt oxide to metallic Co, increases the Co crystallinity, and removes the surfactants to make the surface more active. The authors showed that C–Co represents a very efficient catalyst for the oxygen evolution reaction (OER) in alkaline medium (0.1 M KOH), more active than the commercial Ir catalyst.[203] Moreover, these Co NPs could also be assembled into a well-defined monolayer array on a working electrode using a water–air interface self-assembly method. This allowed the detailed evaluation of their intrinsic OER activity.[204]

Dupont and coworkers have studied the thermal decomposition of $Co_2(CO)_8$ in ionic liquids (ILs) at 150 °C, achieving either the preparation of Co^0 nanocubes or spherical NPs, depending on the type of IL used and the reaction time; after five hours at 150 °C, the initially formed Co nanocubes were completely transformed into irregular Co NPs.[205] The diameter of the nanocubes was 53 ± 22 nm and 79 ± 17 nm for samples prepared in the ILs: 1-*n*-decyl-3-methylimidazolium trifluoro-tris(pentafluoroethane) phosphate ([DMI][FAP]) and 1-*n*-decyl-3-methylimidazolium *N*-bis(trifluoromethanesulfonyl) imidate ([DMI][NTf_2]), respectively. The shape of the cobalt particles was directly related to the self-organisation in the IL and thus could be tuned by modulating the length of the N-alkyl imidazolium side chains, the anion type and the reaction conditions. Noteworthy, the ε-cobalt phase was always observed in all the samples, independent of the reaction time. XRD measurements showed also the absence of cobalt oxide, indicating that a protective layer of the IL around the Co NPs prevents their oxidation.

Another paper by Dupont and coworkers[206] demonstrates that the simple decomposition of $Co_2(CO)_8$ dispersed in imidazolium-based ILs affords superparamagnetic Co NPs having an average size of 5–8 nm, depending on the counter anion. The synthesis of Co NPs was carried out in different ILs, such as 1-*n*-butyl-3-methylimidazolium *N*-bis-(trifluoromethanesulfonyl) imidate ([BMI][NTf_2]), 1-*n*-decyl-3-methylimidazolium tetrafluoroborate ([DMI][BF_4]) or 1-*n*-tetradecyl-3-methylimidazolium *N*-bis(trifluoromethanesulfonyl) imidate ([TDMI][NTf_2]). The morphology and the size distribution of the synthesised particles were analysed by TEM (Figure 7).

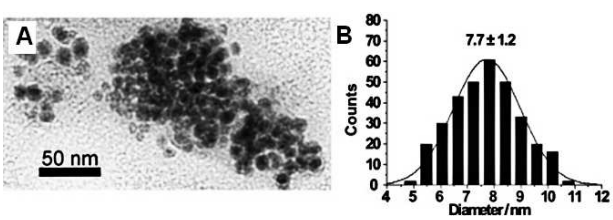

Figure 7. Selected TEM image of Co NPs dispersed in ([BMI][NTf_2] (A). Histogram showing the size distribution of the Co NPs (B). Reproduced from ref. [206].

Monodisperse Co NPs in the size range 3–10 nm can be obtained by the so-called "hot injection" method, namely by thermal decomposition of $Co_2(CO)_8$ at 168–182 °C in the presence of OA, avoiding the use of TOPO, as shown by Somorjai and coworkers (Figure 8).[207] The size of Co NPs can be tuned by careful control of the temperature of the hot OA solution into which the Co precursor is injected. It should be pointed out that monodisperse NPs could be generated without using TOPO, a capping ligand that decomposes under the reaction conditions, giving highly reactive "P" atoms that can phosphatise the metal surface and thus poison the Co catalyst, as shown by the authors.[207]

In the paper of Haumesser and coworkers,[208] Co NPs were successfully synthesised by thermal decomposition of [Co(COE)(COD)] in imidazolium-based ILs under a reducing hydrogen atmosphere at 100 °C. The alkyl chain influences the characteristics of the suspensions and the morphology of the Co NPs. The synthesised Co NPs adopted the non-compact and metastable structure of ε-Co that converted to the stable *hcp* Co NPs at room temperature. The crystalline structure of the isolated Co NPs has been studied in detail by wide angle X-ray scattering (WAXS) and HRTEM (Figure 9). The obtained Co NPs were quite monodisperse with an average diameter less than 5 nm. Their suspensions in ILs were magnetically responsive and were successfully used as ferrofluids, especially under vacuum, thanks to the extreme low volatility of the ILs.[209]

Large-scale synthesis of supported Co NPs was successfully achieved by Park, Yang and coworkers.[210] They used the melt infiltration process, which is an emerging technique that avoids

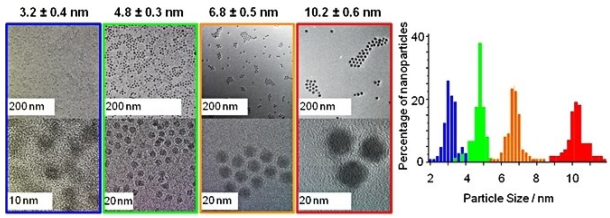

Figure 8. Typical TEM and HRTEM images of particles of four different sizes (3.2, 4.8, 6.8, and 10.2 nm) prepared without using TOPO and controlling particle size by variation of the temperature during the synthesis. Reproduced from ref. [207], Copyright (2012), with permission from the American Chemical Society.

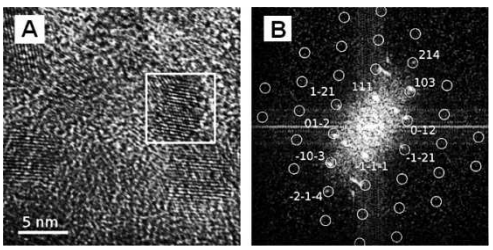

Figure 9. Exemplary HRTEM image of Co NPs generated in [TDMI][NTf_2] (A) and fast-Fourier transform (FFT) analysis of the particle in the white square indexed by a cubic structure along the (−321) zone axis, with a lattice parameter of 0.61 nm corresponding to ε-Co (B). Reproduced from ref. [208], Copyright (2018), with permission from the American Chemical Society.

© 2021 The Authors. European Journal of Inorganic Chemistry published by Wiley-VCH GmbH

the use of additional solvents, and is a fast, convenient route to prepare various supported metal catalysts containing small and well-dispersed active NPs inside robust supports. In their work, $Co(NO_3)_2 \cdot 6H_2O$ was employed as precursor in a simple melt infiltration of the cobalt salt in γ-phase alumina as shown in Scheme 1, and subsequent thermal reduction at 450 °C in a hydrogen flow. TEM inspection showed the successful formation of Co NPs with average size of 15 nm, dispersed on alumina (Co/Al_2O_3), and the X-ray diffraction pattern revealed an *fcc* structure for Co single-crystal domains. The catalytic performance of the resulting Co/Al_2O_3 was evaluated in the Fischer-Tropsch reaction, a relevant industrial process that converts mixtures of CO and H_2 into long-chain hydrocarbons. Co/Al_2O_3 showed promising conversion of CO up to 76% with high hydrocarbon productivity and good stability.

Suh and coworkers synthesised Co NPs by thermal decomposition of the salt cobalt(II) acetate tetrahydrate.[211] Particle size, ranging from 8 to 200 nm in average diameter, was controlled by using various surfactant combinations consisting of trioctylphosphane (TOP), (*Z*)-octadec-9-enylamine (OAm) and OA. XRD patterns of Co NPs coated with various surfactants are shown in Figure 10. Interestingly, all the samples have the same crystalline structure corresponding to the *fcc* crystal phase of bulk metallic cobalt. As the particle size increased from 8 to 200 nm, the peak became sharper, which is a general tendency.[212]

Dong and coworkers reported the synthesis and catalytic application of a nanostructured catalyst based on supported Co

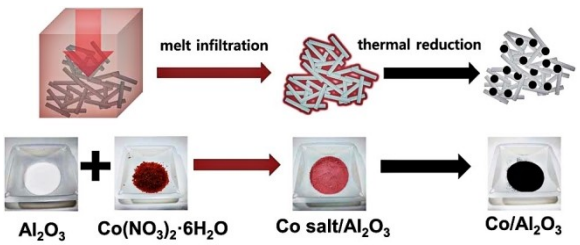

Scheme 1. The facile synthesis of a Co/Al_2O_3 nanocatalyst by melt infiltration and thermal treatment. Reproduced from ref. [210], Copyright (2017), with permission from The Royal Society of Chemistry.

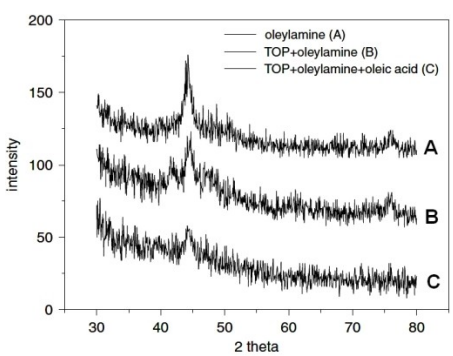

Figure 10. XRD patterns of Co NPs coated with various surfactants. Reproduced from ref. [211], Copyright (2006), with permission from Elsevier.

NPs.[213] The authors synthesised Co NPs supported on *N*-doped mesoporous carbon (Co/mCN-900) by simple one-pot pyrolysis of a homogeneous mixture of melamine, polyacrylonitrile, and $Co(NO_3)_2 \cdot 6H_2O$. The pyrolysis temperature showed a significant influence on morphology and size of the final Co NPs. The optimal pyrolysis temperature for the preparation of the catalyst was 900 °C, named afterwards Co/mCN-900. Very small Co NPs having an average size lower than 6 nm with almost no aggregates were obtained. These Co NPs have a very high number of active sites; this feature in conjunction with the mesoporous fluffy mCN structure that facilitates a high dispersion of Co NPs, contributes to an enhanced catalytic activity. Indeed, Co/mCN-900 was shown to be efficient in the hydrogenation of nitroarenes.[214]

As a variant of this technique, a simple and scalable method based on the high temperature treatment with hydrogen was proposed by Pfefferle and coworkers.[215] Small narrow size distributed Co NPs were deposited inside the pores of single-walled carbon nanotubes (SWCNT) by a two-step procedure. Firstly, SWCNT were heated at 900 °C, then they were filled with a cobalt(II) acetylacetonate solution in dichloromethane by ultrasonication. In the second step, the samples were exposed to hydrogen at high temperature. Results demonstrate that the size and shape of Co particles can be controlled by varying the temperature at which the hydrogen treatment takes place. The reduction of Co^{2+} ions was almost complete at 400 °C, and the Co NPs located inside the SWCNT showed an elongated shape. In contrast, working at 500 °C, the control was lost; large spherical particles were formed and moved from the inner to the outer surface of the nanotubes.

Coville and coworkers presented the size-control synthesis of Co NPs encapsulated inside hollow carbon spheres (HCS) by using polystyrene-*b*-poly(acrylic acid) (PS-*b*-PAA) nanospheres.[216] The latter were prepared from polystyrene spheres by functionalisation with acrylic acid and used for the synthesis of Co_xO_y/polymer composites, which were heated to 600 °C at a rate of 10 °C/min and kept isothermal for 2 h to pyrolyse and carbonise the resorcinol–formaldehyde (RF) forming a carbon shell that encapsulates the Co nanoparticles. It was found that the concentration of poly(acrylic acid) (PAA) in the polymer influences the size of the Co NPs. For instance, Co NPs encapsulated inside HCS (Co@HCS) obtained by using PS-*b*-PAA with 8 mol% of PAA (PS-*b*-PAA_8) and 12 mol% of PAA (PS-*b*-PAA_{12}) have an average size of 5.4 and 6.1 nm, respectively. It should be noted that the Co@HCS involves not only metal NPs, but also oxides of cobalt NPs such as CoO and Co_3O_4, whose variation of composition influences the NPs' size and metal loading.

As shown above, the carbon-based composite is a suitable material in the process of production of Co NPs. A nitrogen-doped carbon was used by S. Liang and C. Liang as nanoshell for the synthesis of encapsulated Co NPs (Co@N-C) via simple decomposition of the solid-phase cyclen-Co-dicyandiamide complex precursor.[217] The structure and properties of NPs can be regulated by the pyrolysis temperature (700–900 °C). It was found that catalysts based on Co@N-C prepared at 800 °C (Co@N-C-800) showed bifunctional catalytic activities for both

© 2021 The Authors. European Journal of Inorganic Chemistry published by Wiley-VCH GmbH

oxygen reduction reaction (ORR) and OER in alkaline electrolyte owing to the nanocomposite's synergetic effect.

Kathiresan, Yun and coworkers have synthesised Co NPs at variable temperatures.[218] Co NPs on ethylene diamine-based porous organic polymers (EPOP) were prepared at 180, 300 and 500 °C (Co-EPOP-HT, Co-EPOP-300 and Co-EPOP-500, respectively). The NPs were stabilised by the amine groups on the porous organic polymers. The Co-EPOP-based nanocatalytic systems were tested in water-splitting reactions, i.e. OER and hydrogen evolution reaction (HER), and showed effective electrocatalytic activity, which was compared to Co NPs catalyst without polymer support. The HER activity of the catalysts were in the order Co-EPOP-500 > Co-EPOP-300 > Co-EPOP-HT > Co NPs. It should be noted that the Co-EPOP-based electrocatalysts exhibited excellent stability under acidic and basic conditions.

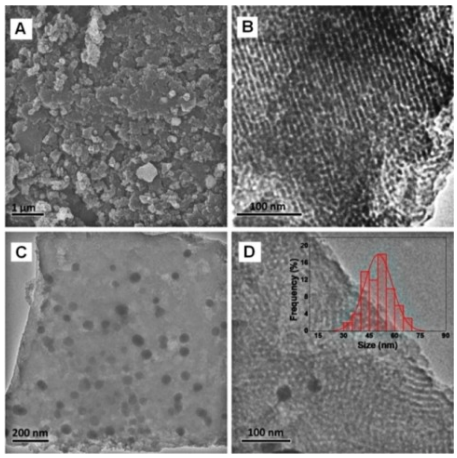

Figure 11. SEM image of CoNPs@OMC (A), TEM images of OMC (B) and CoNPs@OMC (C, D). The inset in (D) is the particle size distribution of the Co NPs in CoNPs@OMC. Reproduced from ref. [220], Copyright (2017), with permission from Elsevier.

4.3. Hydrothermal and solvothermal syntheses

A relevant concern in the preparation of NPs is the control of NPs growth. Hydrothermal synthesis can be seen as a variant of the synthesis of Co NPs by thermal decomposition, and proceeds in aqueous solution under pressure and at elevated temperatures, far above the boiling point of water. The reagents are placed in a certain amount of water and then heated to high temperature in a closed vessel. The particle size and form can be controlled by tuning the experimental conditions, such as temperature, pH, and pressure. The difference between solvothermal and hydrothermal method is the use of organic media such as alcohols, amines or ILs in the first case, instead of an aqueous solution as in the latter case.[219]

Based on this technique, Liu and coworkers have successfully developed a novel composite CoNPs@OMC, where OMC = ordered mesoporous carbon, with Co NPs homogeneously embedded or confined in the ordered mesoporous carbon, by a simple one-step carbonisation/reduction assisted by a previous hydrothermal process.[220] The latter was carried out by heating a mixture of $Co(NO_3)_2 \cdot 6H_2O$, formaldehyde, hydrochloric acid and a suitable copolymer in water at 100 °C for 10 h. The subsequent carbonisation was conducted under argon atmosphere at 600 °C for 3 h. The resulting CoNPs@OMC composite showed a deteriorated ordered mesoporous structure (Figure 11), which is consistent with the XRD analysis. On the basis of TEM measurements, the particle size distribution for CoNPs@OMC composite is in the range of 30–75 nm and the average particle size is 49.4 nm which is larger than the grain size calculated by the Scherrer equation, implying that the Co NPs are polycrystalline.

Lee and coworkers synthesised Co NPs using $Co(NO_3)_2$ as precursor without any stabiliser in supercritical methanol. The reaction proceeded through the formation of cobalt methoxynitrate at an initial stage, which was then converted to CoO and finally reduced to metallic Co.[221] In practice, methanol plays a role both as reaction medium and as reducing agent. The fast formation of crystalline Co NPs within 15 min is due to high reaction temperatures and pressure. Superconducting quantum interference device (SQUID) measurements confirmed ferromagnetic behaviour for the synthesised Co NPs.

It is well known that Co NPs are rather sensitive to oxidation in ambient conditions; therefore, one of the major problems to be faced during their preparation is to avoid oxidation. Seong and Adschiri tried to solve the problem by using a hydrothermal synthesis based on two tandem reactions, first formation and later reduction of cobalt monoxide.[222] It is worth noting that the proposed reaction mechanism, shown in Scheme 2, was derived from kinetic analysis, assuming a first-order irreversible reaction.

Datta and coworkers prepared Co NPs-reduced graphene oxide (Co-RGO) nanocomposites with different shape of NPs depending on the synthesis techniques.[223] They obtained cube-shaped Co-RGO (10 nm) by hydrothermal method at non-equilibrium conditions at 90 °C, spherical Co-RGO (6 nm) by co-precipitation method at room temperature and rod-like Co-RGO (123 nm length, 6 nm width) by applied magnetic field with co-precipitation; the size was measured by TEM. The magnetic

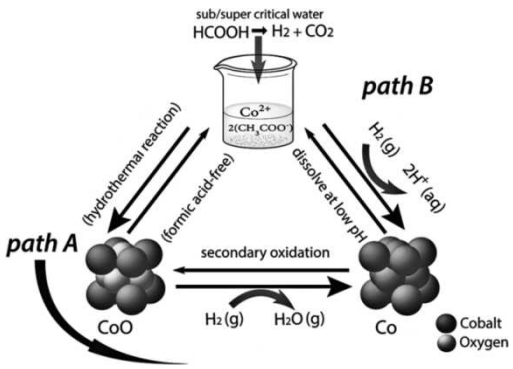

Scheme 2. The proposed reaction mechanism for formation of Co NPs in the reductive supercritical hydrothermal process. Reproduced from ref. [222], Copyrght (2014), with permission from The Royal Society of Chemistry.

© 2021 The Authors. European Journal of Inorganic Chemistry published by Wiley-VCH GmbH

study carried out with temperature gradient showed a transition from ferromagnetic to superparamagnetic behaviour; cube-shaped Co-RGO had the highest values for magnetic parameters, such as coercivity and magnetic moment.

4.4. Reduction of cobalt salts

The "wet chemical" reduction has become the most common method in the preparation of metal NPs. It is based on the use of a reducing agent, such as hydrogen, alcohol (see for details Section 4.5 on the polyol process), hydrazine or borohydride, that is mixed with the metal salt in the presence of a stabilising agent (ligands, polymers, dendrimers, surfactants) to prevent formation of metal powders and agglomeration. Thus, the actual size of NPs depends on many factors, such as type of reducing agent, metal salt, solvent, concentration, temperature, and reaction time. It should be noted that capping agents play an important role in the production of NPs.[224] The stabilisers control and regulate the growth of nanoparticles and prevent their aggregation. Various types of capping agents, including surfactants, ligands, polymers, dendrimers, cyclodextrins, etc., have been used in colloidal synthesis.[225,226]

Sun and Murray synthesised magnetic colloidal ferrofluids based on crystalline Co NPs by reduction of cobalt(II) chloride with lithium triethylborohydride (superhydride) in the presence of stabilising agents.[227] The combination of OA and TOP was used for both growth control and steric stabilisation. The Co NPs possessed the unstable *ε*-Co structure and could be transformed quantitatively to the common *hcp* phase by annealing at 300 °C (Figure 12). It should be noted that the deposition of uniform Co NPs on solid substrates by evaporation of the carrier solvent resulted in the spontaneous assembly of two-dimensional and three-dimensional magnetic colloidal crystals.[228]

An easy method to prepare *hcp* Co NPs was proposed by Zhang and coworkers[229] using for the first time *N,N*-dimethylformamide (DMF) both as solvent and reducing reagent. The reaction, carried out at 160 °C for 12 h, involved the oxidation of DMF to carboxylic acid as well as the reduction of Co^{2+} to Co^0. TEM micrographs of the isolated Co NPs showed an average diameter of 6 nm, and the selected area electron diffraction (SAED) pattern indicated a polycrystalline nature.

In the work of Dravid and coworkers, Co NPs were synthesised using OA as surfactant and TOP as reducing agent keeping the reaction mixture at 250 °C for 30 min.[230] Infrared spectroscopy and XPS indicated that OA molecules were chemisorbed on the surface of the particles as carboxylate forming a covalent Co–O bond. In this way, a stable colloidal solution was formed. Figure 13 shows TEM micrographs of Co NPs coated with OA. The particle size is about 15–20 nm.[230]

In another interesting work by Petit and coworkers, OA was simultaneously used as the reducing agent, solvent and surfactant.[231] The authors described a one-pot synthesis of pure mono-disperse crystalline ferromagnetic *hcp* Co NPs by chemical reduction of cobalt(I) complex $[CoCl(PPh_3)_3]$ using OA at 190 °C. A possibility to control and tune the shape (spheres or rods) and the size of Co NPs by varying the concentration and the reaction time has been shown. For example, a morphological transition occured from spheres to rods on increasing the reaction time of the synthesis. The ferromagnetic behavior of Co NPs even at room temperature was confirmed by SQUID measurements. Moreover, the authors recently investigated the role of the OA in the mechanism of formation of *hcp* Co NPs by theoretical and experimental studies.[232] It was demonstrated that OA plays a key role in both the kinetics and the thermodynamics of the disproportionation.

Alex and coworkers introduced an easy and inexpensive chemical method in alkaline medium for the preparation of pure Co NPs at ambient temperature, which was completed instantaneous without employing additional nucleating agent.[233] The results indicated the formation of smaller particles with an increase in concentration of cobalt ions in solution and dominance of *fcc* cobalt on reduction at room temperature. The particle size of 50–70 nm was determined by TEM, but XRD analysis by the Scherrer formula gave a size around 24–49 nm.

Salman and coworkers investigated the synthesis and formation mechanism of Co NPs[234] prepared at room temperature using $CoSO_4 \cdot 7H_2O$ as precursor and aqueous hydrazine as reducing agent. The influence of the reaction parameters was studied with the help of anode and cathode polarisation experiments. A higher reducing power of N_2H_4 was observed at high pH in agreement with the known process of oxidation of

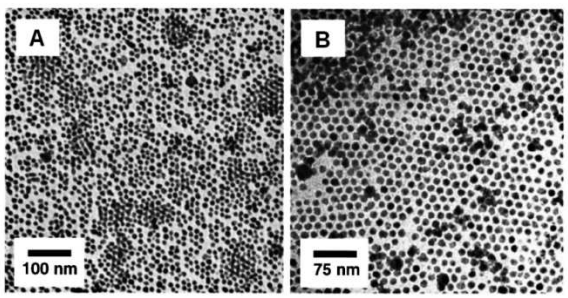

Figure 12. TEM micrographs of *hcp* Co NPs derived from annealed *ε*-Co NPs at 300 °C (A) and cobalt oxide NPs from oxidation of the annealed Co NPs (B). Reproduced from ref. [227], Copyright (1999), with permission from the American Institute of Physics.

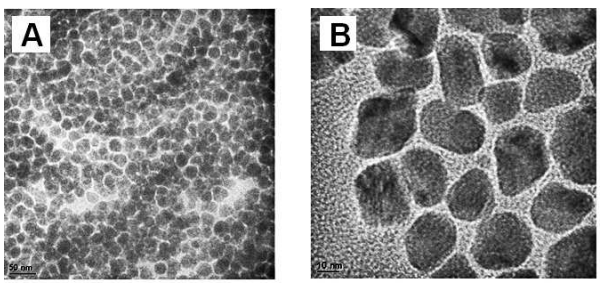

Figure 13. TEM micrographs Co NPs (A), high magnification image of Co NPs (B). Reproduced from ref. [230], Copyright (2004), with permission from the American Chemical Society.

© 2021 The Authors. European Journal of Inorganic Chemistry published by Wiley-VCH GmbH

hydrazine to nitrogen that consumes OH^-. Thus, the reduction of cobalt(II) sulfate was performed at pH 14. Interestingly, the addition of citric acid, largely used by many groups as capping agent to protect and stabilise metal NPs, also increased the reducing power of hydrazine. The so-obtained Co NPs had a spherical shape with a very large diameter of 400 nm. When the concentration of hydrazine in the reaction mixture was lower than 5 M, its diffusion was slow and the Co crystals grew in one direction, thus formation of dendritic Co NPs was observed, both at room temperature and at 80 °C.

Guo and coworkers prepared Co NPs in an ethanol/hydrazine/alkaline system at room temperature. The reaction was completed instantaneously, and the isolated NPs were characterised by XRD, TEM, and differential thermal analysis (DTA).[235] Interestingly, when the NPs were heated in argon at 200 °C for 2 h, the *hcp* phase of Co NPs grew more regular and larger, and the coercivity of the sample increased from 480 to 680 Oe.

It is well known that sodium borohydride is a powerful reducing reagent and was intensively used for the reduction of metal ions to NPs. The studies by Klabunde and coworkers[169,170] have shown that the nature of the final products formed by reduction with $NaBH_4$ depends on the solvents. Thus, preparation of Co NPs in aqueous solution usually gives cobalt borides rather than the pure metal.

Kamal and coworkers described the synthesis of Co NPs supported on natural polymers such as cellulose and chitosan.[236] These two macromolecules have the advantage to be biocompatible and abundant in nature; moreover, they possess functional groups on the surface, such as –OH (cellulose) and both –OH and $–NH_2$ groups (chitosan), which can coordinate metal atoms through their lone pair of electrons. A hydrophilic chitosan was used to improve the metal deposition on the polymer. Thus, cellulose microfibres of filter paper were coated with 1 wt% of chitosan followed by adsorption of an aqueous Co^{2+} solution. Subsequently, the material was dipped into a 0.19 M sodium borohydride solution to accomplish the reduction. The determination of the amount of Co NPs present on the support and the thermal properties were measured by thermogravimetric analysis (TGA). The supported Co NPs were applied as heterogeneous catalyst in the hydrogenation of 2,6-dinitrophenol, a highly toxic water pollutant. The catalyst proved to be efficient and stable after four consecutive runs.[236]

Starch hydrogel-loaded Co NPs were prepared by *in situ* reduction of Co^{2+} ions on a starch hydrogel network.[237] Co NPs with a spherical-like shape and size of 30 nm were obtained. The prepared nanocomposite was applied as heterogeneous catalyst in the reaction of hydrogen production from the hydrolysis of $NaBH_4$. The starch hydrogel-loaded Co NPs showed high catalytic activity which was maintained over five catalytic runs.

Thiols, carboxylic acids and amine-based capping agents are widely used in the stabilisation of Co NPs, while macrocycles like phthalocyanine and porphyrines have been rarely used for this purpose. One example has been reported by Sannegowda and coworkers who prepared Co NPs using the macrocycle tetraaminephthalocyanine (TAP) as a stabilising agent.[238] It was observed that, once dispersed in dimethyl sulfoxide (DMSO), the NPs showed a spherical shape and an average diameter of 3 nm, while the dispersion of the same NPs in ethanol suffered from aggregation and a pearl-chain structure was formed. This was attributed to the magnetic dipolar interaction between neighbouring particles that was stronger in the presence of a less coordinating solvent such as ethanol. If NPs obtained from ethanol were re-dispersed in DMSO, the chain-like structure broke down to give a uniform distribution of spherical NPs. Surface enhanced Raman spectroscopy (SERS) was 100 times more intense in an ethanol dispersion compared to DMSO. Noteworthy, the macrocycle TAP was more efficient in the stabilisation of NPs in comparison to common capping agents and prevented the formation of an oxide layer for a week.

Pileni and coworkers reported the synthesis of Co NPs of 5.8 nm in reverse micelles based on chemical reduction of $[Co(AOT)_2]$ (AOT = bis(2-ethylhexyl)sulfosuccinate) by $NaBH_4$.[239,240] The formation of *fcc* Co NPs was detected by TEM (Figure 14), small angle X-ray scattering (SAXS) and EDX analysis. Noteworthy, these Co NPs in a 2D self-assembled hexagonal network are stable in air and have a narrow size distribution.

In another paper, Lisiecki and Pileni produced crystalline Co NPs in $[Co(AOT)_2]$ reverse micelles.[241] The micelles and a low volume of reducing agent play the role of nanoreactors for the nucleation and growth of Co NPs. The authors demonstrated that the amount of reducing agent is one of the key parameters in controlling the size distribution of nanocrystals and observed a slight difference in average particle size. With a suitable $[NaBH_4]/[Co(AOT)_2]$ molar ratio, they could obtain organisations of NPs in compact hexagonal networks.

Xiao and coworkers reported a modification of the chemical reduction method based on the use of $NaBH_4$ to produce homogeneous spherical Co NPs with a narrow size distribution.[242] The traditional method was modified by adding a layer of mineral oil to the ethanol solution of $CoCl_2$ and by subsequently dropwise addition of $NaBH_4$ in ethanol. In this

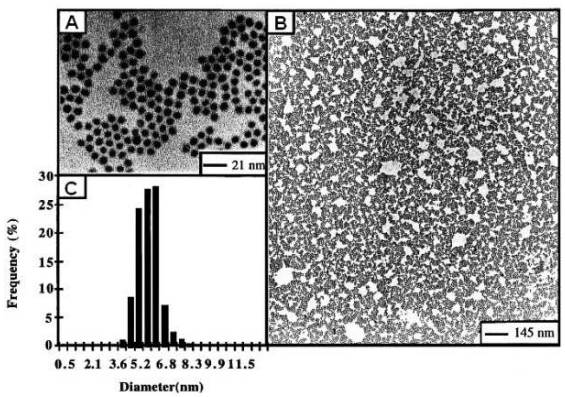

Figure 14. TEM patterns at different magnifications (A, B) and histogram of the size (C) of the ordered hexagonal monolayers of Co NPs. Reproduced from ref. [239], Copyright (1999), with permission from the American Chemical Society.

© 2021 The Authors. European Journal of Inorganic Chemistry published by Wiley-VCH GmbH

way, it was possible to control the particle nucleation and growth by immediately removing the formed particles from the reaction site. From data of TEM analysis, the average particle size is around 4.7 nm with standard deviation of 1.6 nm.

Using as solvent ethanol instead of water, they could also minimise the formation of metal borides and metal oxides. It is known that especially in the case of Fe, Co and Ni, the reduction of the metal salts with $NaBH_4$ gives rise to transition metal borides rather than pure metals.

The possibility of forming hexagonal Co NPs with high saturation magnetisation by direct chemical synthesis was explored by Abel and coworkers.[243] The NPs were synthesised by reduction of anhydrous cobalt(II) chloride with $NaBH_4$ in 2,5,8,11,14-pentaoxapentadecane (tetraglyme) at temperatures in the range of 200–270 °C under a nitrogen–hydrogen atmosphere and controlled by the addition of different surfactants. The as-made particles were further annealed under a 5 % H_2/95 % Ar atmosphere to improve their properties. So far, the best magnetic properties were obtained for spherical *hcp* Co NPs with an average size of 45 nm, a saturation magnetisation of 143 emu g^{-1} and coercivity of 500 Oe. The saturation magnetisation and coercivity were further improved by annealing the Co NPs, leading to a saturation magnetisation of 160 emu g^{-1} and coercivity of 540 Oe (Figure 15).

Garbarino and coworkers[244] studied the *ex situ* production of Co-based NPs immobilised on α-Al_2O_3 and using cobalt-containing materials as catalysts for ethanol steam reforming (ESR).[245] Firstly, Co NPs were obtained by reduction of $CoCl_2 \cdot 6H_2O$ with sodium borohydride and were afterwards mixed with α-Al_2O_3 either by mechanical mixing or by sonication in the presence of an organic volatile solvent and under argon flux, followed by annealing at 500 °C. The Co-based NPs are characterised by a fully amorphous phase where the globular particles have a size less than 50 nm. The nanostructured catalyst, prepared by mechanical mixing, was applied for the production of hydrogen through ESR and gave satisfactory results.

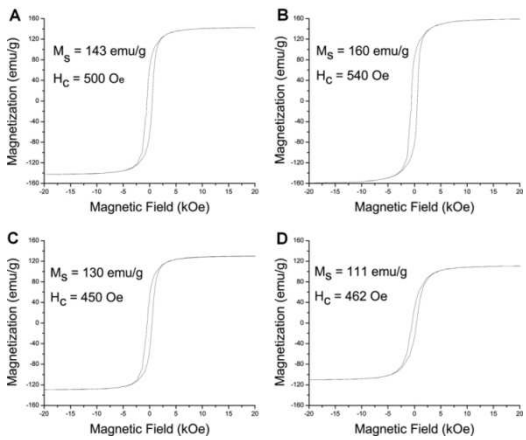

Figure 15. Hysteresis loops from Co NPs synthesised in different surfactants, namely OA (A), annealed OA sample (B), OAm (C), and PVP (D) at room temperature. Reproduced from ref. [243], Copyright (2016), with permission from Elsevier.

Busca and coworkers also reported the synthesis, characterisation and application of Co NPs as catalyst.[246] The latter have been prepared by reduction of $CoCl_2 \cdot 6H_2O$ by sodium borohydride in aqueous solution producing first very small particles with average diameter 5–6 nm that afterwards formed bigger spherical, amorphous, and superparamagnetic aggregates. Structural characterisation was carried out using XRD, morphological studies were performed with field emission scanning electron microscopy (FE-SEM). Co NPs crystallised in the cubic structure, which is confirmed by annealing at 500 °C.

Another paper about catalytic application of Co NPs was published by Mahdavi and coworkers.[247] The authors reported the synthesis and characterisation of Co NPs-decorated multi-walled carbon nanotubes (Co/MWCNTs) that were afterwards embedded in a polymeric membrane. Co NPs were grown on the surface of MWCNTs by reduction of $CoCl_2 \cdot 6H_2O$ with sodium borohydride and L-ascorbic acid (L-AA) at room temperature and were obtained in the size range of 50–70 nm and with a good dispersion without any agglomeration. Catalytic membranes incorporating Co NPs showed a good catalytic activity for the reduction of 4-nitrophenol to 4-aminophenol (conversion 100 %).

The work of Zola and coworkers addressed the preparation of Co NPs using three different methods, (i) thermal decomposition of $Co_2(CO)_8$, (ii) the polyol process, and (iii) the reduction of cobalt salt by borohydride.[248] The case (i) was the most appropriate to control size and shape by modification of the molar ratio precursor/surfactant, giving spherical NPs with low size distribution. In the polyol process (ii), working at high temperatures, undefined-shape NPs were formed; on adjusting the TOP/OA ratio, spherical NPs were obtained. In the last method (iii), the amount of reducing agents, i.e. $NaBH_4$, has a key role in the size distribution of the NPs, and by adjusting the $NaBH_4$/precursor ratio, spherical NPs with size 3.64 ± 0.64 nm were obtained.

4.5. The polyol process

One of the most promising methods for the synthesis of uniform Co NPs is the polyol process. A huge number of publications is devoted to the preparation of Co NPs by this method, which is characterised by mild (low temperature, normal pressure) and ecologically friendly conditions.

The polyol, being a high boiling liquid, acts as a solvent for the metal precursor (usually a metal salt), as a reducing agent, and in some cases, as a complexing agent for the metal cations.[249,250] There is a great advantage in this method, because when reducing agents such as borohydrides are used (see Section 4.4), these and the stabilising agents can pollute the surface of NPs and induce their aggregation. Thus, using the polyol process, these drawbacks can be avoided. From a mechanistic point of view, the polyol process is based on the dehydration and oxidation of the alcohol to aldehydes or ketones (depending on the nature of the polyol used), and this process promotes the reduction of Co ions to Co metal.[251,252] Thus, a proper choice of the polyol is important, having the

© 2021 The Authors. European Journal of Inorganic Chemistry published by Wiley-VCH GmbH

reducing potential suitable to carry out the reduction of the cobalt precursor. It has been shown that increasing the temperature and pH of the reaction mixture increase the rate of the overall reaction.[253] While the reduction of metal salts with borohydride is very fast, occurring at room temperature and producing relatively small NPs, the reduction using polyol is usually slow. Thus, to achieve small Co NPs with size 2–20 nm, either surfactants or heterogeneous nucleation agents such as Pt or Pd are used. An understanding of the reaction path during the reduction of metal ions by polyols is necessary to design better processes for the synthesis of metal NPs with desired shape and size. In a paper by Jeyadevan and coworkers, a detailed study was performed aiming at understanding the influence of polyol, the kind of metal salts, and additives such as OH^- ions in the formation of metal NPs.[254] The cobalt salts, once dissolved in polyol, were found to undergo the formation of cobalt complexes, cobalt alkoxides or cobalt hydroxides, depending on the metal salt precursor and on the presence of hydroxide anions. Afterwards, the reduction of the *in situ* formed cobalt(II) derivative coming from cobalt(II) acetate tetrahydrate $Co(OAc)_2 \cdot 4H_2O$ or cobalt(II) chloride hexahydrate $CoCl_2 \cdot 6H_2O$ led to the formation of Co NPs. The reaction giving the metal complexes is relevant since it was found to determine the physical properties of the NPs. The reaction rate was enhanced in the presence of hydroxide anions by accelerating the oxidation of polyol. SEM micrographs of the intermediate precipitate obtained by the polyol process are shown in Figure 16.

In another work, a detailed investigation of the mechanism by which Co NPs are formed using cobalt(II)-ethylene glycole (EG) was reported.[255] The structural and spectral analyses such as XRD, nuclear magnetic resonance (NMR), Fourier-transform infrared spectroscopy (FTIR) and electrospray ionisation time-of-flight mass spectrometry (ESI-TOF-MS) were used for monitoring

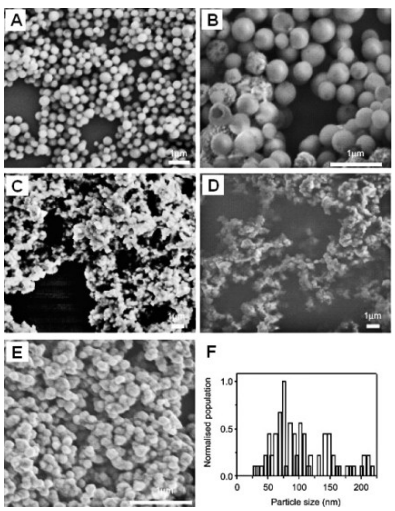

Figure 16. The SEM micrographs of the intermediate precipitate obtained in EG without OH^- at 200 °C/15 min (A), 200 °C/40 min (B), and with OH^- at 180 °C (C), 190 °C (D); cobalt particles at 195 °C (E) and their corresponding particle size distribution (F). Reproduced from ref. [254], Copyright (2007), with permission from Elsevier.

and identifying the products formed during the redox process. At the first stage, the formation of monoanionic $E\bar{G}$ takes place in the presence of a base (metallic Na or NaOH, or sodium acetate). This results in the formation of intermediate cobalt(II) glycolate that undergoes fast reduction to Co^0 with oxidation of the monoanionic $E\bar{G}$ to acetaldehyde. Finally, an overall redox scheme was proposed based on the experimental observations. This study could be widely used for the preparation of metal and alloy NPs using polyols or alcohols.

W.-T. Cheng and H.W. Cheng used the microwave-assisted polyol method in the presence of PVP as capping agent (12 times molar amount with respect to cobalt(II) acetate) and $PdCl_2$ that, being a microcrystalline salt, works as seeds for nucleation.[256] The reaction was carried out at 175 ± 10 °C and the maximum yields of synthesised Co NPs with average diameter 40 and 81 nm from reduction of 0.1 and 0.075 M of cobalt(II) acetate were about 71 and 85 %, respectively. XRD was used to characterise the structure of the synthesised Co NPs. Furthermore, the as-synthesised Co NPs dispersed in kerosene showed a superparamagnetic behaviour at room temperature, while Co NPs with an average size of 109 nm showed a cohesive character.

The synthesis of Co NPs by a modified polyol process has been described by Sekhar and coworkers.[257] The novelty introduced was the reducing agent, hydrazine in boiling EG at 190 °C, that allowed much shorter reaction times, i.e. 30 minutes instead of 4 hours, in comparison to the traditional polyol process.[258] The main advantage of this method is the preparation of oxide-free Co NPs. The particle size, as shown by TEM analysis, could be varied by the amount of PVP, going from 200 nm diameter in the absence of PVP, to 35 nm diameter in the presence of PVP. Additionally, when the size of the Co NPs decreases, the magnetisation also decreases while the coercivity is strongly increased. Accordingly, Co NPs with a size of 35 nm show the highest coercivity (109 Oe), which is very interesting from the viewpoint of possible applications in magnetic recording media.

Simakova and coworkers synthesised colloidal Co NPs by a modified polyol method using sodium borohydride as a reducing agent.[259] The influence of the gas atmosphere, either inert or oxidative, and of the reduction temperature on formation of NPs was studied. A series of Co NPs having average diameter ranging from 1.8 to 2.8 nm were obtained by varying the conditions. In order to find out the best operating parameters to achieve a controllable formation of Co NPs, the role of the reduction temperature under an inert gas atmosphere was investigated. Changes in the reduction temperature affected the reduction rate and, thus, allowed particle size regulation.

Balela and coworkers reported a facile low-temperature synthesis of colloidal Co NPs by reduction of $CoCl_2 \cdot 6H_2O$ in EG.[253] The obtained colloidal particles were spherical and monodispersed with an average diameter of 2–7 nm. It should be pointed out that pH, reaction temperature and molar ratio of N_2H_4 to Co^{2+} influenced the reduction rate. An alkaline medium, a temperature around 80 °C, and high molar ratios of N_2H_4 to Co^{2+} promoted the formation of colloidal Co NPs. The

© 2021 The Authors. European Journal of Inorganic Chemistry published by Wiley-VCH GmbH

authors also described the precipitation of the NPs which resulted in weakly agglomerated spherical Co structures of submicron size. XRD of the obtained powder showed an *hcp* structure for cobalt.

In 2017,[260] Piquemal and coworkers reported the quantitative study of the influence of the stirring rate on the structural, morphological, and magnetic properties of anisotropic Co NPs, which were prepared by the polyol process using long-chain carboxylates as shape-directing agents. It was shown that the stirring rate has to be carefully controlled within a very small range (about 50–200 rpm) to ensure the production of ferromagnetic pure *hcp* rod-shaped Co NPs displaying low stacking fault densities, high aspect ratios, well-defined crystal habits and high coercivities. In the case of high agitation speed, the Co NPs displayed a marked surface roughness associated with high stacking fault densities and reduced coercive fields. The authors proposed a mechanism to explain the different morphologies observed. High stirring speeds would cause a local disorganisation of the carboxylate ligand layers which in turn contributes to an easier access of the Co monomers to the metal surface leading to a growth direction perpendicular to the long axis of the particles. Thus, the influence of reaction parameters (i.e. nature of the metal precursors, nature of the polyol, basicity of the medium, stirring rate) exerts a significant impact on the crystal habit. The resulting magnetic properties are strongly related to the morphological and micro-structural properties of the prepared rod-shaped NPs.

A follow-up of this study was published in 2019[261] by Piquemal and coworkers who envisaged a one-step seed-mediated polyol synthesis of Co NPs, which is based on the heterogeneous nucleation of *in situ* generated seeds. Either iridium(III) or ruthenium(III) chloride were used as the nucleating agent for the synthesis of Co NPs by reduction of cobalt carboxylate in liquid polyols. The prepared Co NPs have a size of 15–50 nm and show different shapes such as rods, platelets and hourglass-like particles which can be finely tuned by varying the seed structures. The data of geometrical phase analysis allowed to determine the epitaxial growth of the *hcp* Co NPs on *fcc* Ir or *hcp* Ru seeds.

Rodriguez-Gattorno and coworkers reported a comparative study of four different protocols that afforded cobalt microparticles (MPs) and NPs.[262] The synthesis in aqueous media employing borohydride (stronger reductant than hydrazine) offers a convenient route to obtain Co NPs with size of 2 nm, but with lesser purity in comparison with hydrazine as reducing agent. Another method was the reduction achieved by the polyol process (hydrazine in EG) which in turn gave bigger particle sizes that agglomerate in secondary MPs (0.5 μm to 1.5 μm) with spherical shapes. Hollow elongated mesoscopic microstructures can be obtained by using hexadecyl(trimethyl)-ammonium bromide (CTAB), while in the presence of sodium citrate the secondary MPs are solid and not organised.

4.6. Electrochemical methods

Chemical methods for the synthesis of Co NPs have the advantage of being the simplest, most convenient, available, and effective methods. Despite this, there are a number of rather serious limitations. Most chemical methods are based on redox reactions driven by a reducing agent like sodium borohydride, sodium citrate, H_2 gas, amines or hydrazine and the formed by-products pollute the NPs' surface. It is known that Co NPs have unique catalytic, magnetic, and optical properties, but the mentioned limitations of chemical methods lead to a decrease in these properties due to defects formed on the surface of the NPs, and thus impose restrictions on their practical use in catalytic processes.

In the last decades, electrochemical methods have become more and more popular in synthetic chemistry, due to the use of the universal reagent – the electron. After the pioneering work of Reetz and Helbig in the 1990s,[263] the electrochemical synthesis of metal NPs has flourished and represents nowadays one of the most promising methods.[264] The process is characterised by mild conditions, one-step operation, selectivity and application of a convenient and relatively inexpensive type of energy, namely electricity.

The electrochemical route avoids the use of reducing agents, whose by-products may contaminate the NPs; thus, the highest purity can be achieved. Further advantages of electrochemical synthesis are the experimental accessibility and the ability to control the growth of NPs. By tuning electron density, it is possible to control the particle size – high current density leads to small NPs and vice versa. The particle size can also be controlled by adjusting the distance between the electrodes and other common parameters, such as reaction time, temperature, or solvent polarity.

Electrochemical processes applied to the production of nanoscale colloidal metal particles have been recently reviewed.[265–268]

Gonzalez and coworkers presented the study of nanostructured cobalt clusters which were generated by an electrochemical method.[269] This method is based on the cobalt anode oxidation followed by migration of the generated cations to the cathode, where they are reduced back to the zero-oxidation state forming metal atoms adsorbed on the surface (adatoms). The four-electrode cell, formed by a cobalt anode (sacrificial electrode), two platinum cathodes and a platinum pseudo-reference electrode, was used for the synthesis; the electrolytic solution was used as the stabilising agent. The nanoclusters obtained without stirring have spherical shape, while the ones obtained with stirring show a needle shape with particle size of 2–10 nm. The electrochemical method is a quick and clean way to obtain metal NPs.

Ledo-Suarez and coworkers described the electrochemical preparation of Co NPs with size 2–5 nm in diameter.[270] The electrosynthesis was carried out in the presence of a tetraalkylammonium salt as electrolyte. Fine-tuning of the particle size in the nanometre region was obtained by adjustment of the current density. A fatty acid OA and TPP were used to ensure stabilisation of the colloidal NPs. It is noteworthy that the

© 2021 The Authors. European Journal of Inorganic Chemistry published by Wiley-VCH GmbH

colloidal system was stable against oxidation once suspended in *n*-heptane. TEM analysis showed the formation of Co NPs of about 2 nm that can be associated with Co_{309} clusters corresponding to a four shell compact structure, having 162 atoms in the last surface shell.

Schiavi, Altimari and coworkers carried out an in-depth study of the electrochemical deposition of Co NPs and cobalt microstructures onto aluminium foils.[271–274] The study of the electrochemical nucleation and growth processes of cobalt on aluminium was performed by cyclic voltammetry (CV). The increasing amount of charge resulted in an increase of the mean size and a limited decrease in number density of the NPs, probably due to the formation of aggregates.

The research group of Yanilkin investigated the anthracene-mediated electrochemical synthesis of Co NPs in solution.[275] The synthesis of Co NPs was performed by using anthracene as a mediator in the electrolysis at the potential of anthracene reduction to the radical anion in aprotic DMF and generating $[CoCl_4]^{2-}$ ions by dissolving the bulk cobalt anode during the electrolysis (Scheme 3). It is important to note that the cobalt particles are oxidised upon contact with air forming oxidised Co NPs with a low dispersity (20–30 nm). The investigation was carried out using CV, electrolysis, dynamic light scattering (DLS) and SEM.

In 2018, we have reported the electrochemical generation of superparamagnetic Co NPs.[276] The electrochemical reduction of cobalt dibromide 2,2′-bipyridine (bpy) complexes (Co/bpy molar ratio 1:0.5–1) results in the formation of Co NPs due to a disproportionation reaction of the electrochemically generated cobalt(I) mononuclear complexes (Scheme 4).

The investigation of the process of electrochemical generation of Co NPs was carried out by CV, macroscale electrolysis, and *in situ* electron paramagnetic resonance (EPR) spectroelectrochemistry (Figure 17).

According to SAXS analysis, the average diameter and the average length of the electrochemically formed cylindrical Co NPs varied from 9 to 10 nm and 30 to 32 nm, respectively, and was correlated with the *g* value and the broadness of the ferromagnetic resonance (FMR) signal observed by *in situ* EPR-spectroelectrochemistry during the electrochemical process.

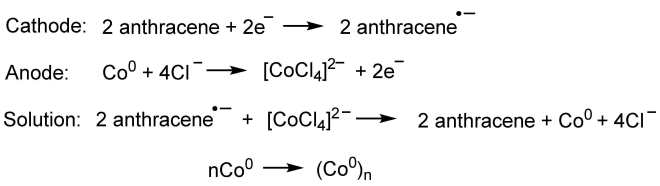

Scheme 3. The electrosynthesis of Co NPs $(Co^0)_n$ using anthracene as a mediator and a cobalt anode as a supplier of Co^{2+}.

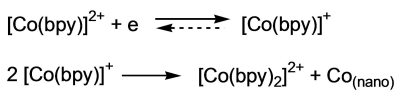

Scheme 4. The preparation of Co NPs. Reproduced from ref. [276], Copyright (2018), with permission from Elsevier.

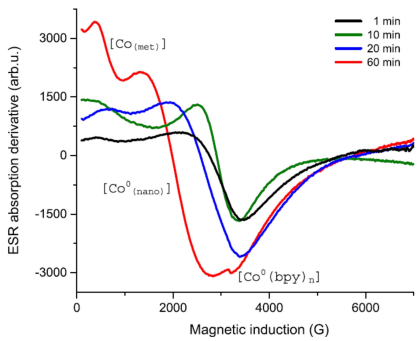

Figure 17. EPR spectra recorded from a solution containing electrochemically generated Co NPs measured in a combined EPR-electrochemical cell after 1, 10, 20 and 60 min of electrolysis. Reproduced from ref. [276], Copyright (2018), with permission from Elsevier.

5. Summary and Outlook

Co NPs have great scientific and technological relevance, due to their catalytic, magnetic, electronic, and optical properties that are also observed in their composites. Furthermore, cobalt is a biologically active and non-toxic element, which allows its application in the biomedical field, as well as in the context of green chemistry. The synthesis of Co NPs can be carried out in many different ways; the principal routes can be summarised as follows: (i) chemical reduction of cobalt salts, (ii) thermal decomposition of an organometallic precursor, and (iii) the polyol process. The literature discussed in this review highlights the advantages and limitations of each route. The physical methods, as for instance laser ablation, are characterised by simpler process execution but require special equipment and also show a lack of size control for particles smaller than 100 nm.

In general, the synthesis of Co NPs by chemical reduction represents the easiest way to control composition, size, and shape of NPs and to perform a scale-up, without requiring special lab equipment or conditions. However, it suffers from several limitations dealing with the preparation of chemically pure and clean nanoparticles without contamination of the surface layer by reagents and side products. On the other hand, the thermal decomposition leads to issues in controlling the chemical composition of the final NPs. Electrochemical techniques overcome these drawbacks and allow a selective and clean generation of NPs, thus offering significant future perspectives.

List of abbreviations

AFM	atomic force microscopy
AOT	bis(2-ethylhexyl)sulfosuccinate
bpy	2,2′-bipyridine
C–Co NPs	cobalt nanoparticles loaded on Ketjen carbon

© 2021 The Authors. European Journal of Inorganic Chemistry published by Wiley-VCH GmbH

C–V	capacitance–voltage
Co/mCN	cobalt nanoparticles on *N*-doped mesoporous carbon
Co/MWCNTs	cobalt nanoparticles on multi-walled carbon nanotubes
Co/N-CNFs	cobalt nanoparticles on *N*-doped carbon nanofibres
Co@HCS	cobalt nanoparticles encapsulated inside hollow carbon spheres
Co@N-C	cobalt nanoparticles encapsulated inside *N*-doped carbon
Co-RGO	cobalt nanoparticles on reduced graphene oxide
COD	cycloocta-1,5-diene
COE	cyclooctenyl
CTAB	hexadecyl(trimethyl)ammonium bromide
CV	cyclic voltammetry
DC	direct current
diglyme	1-methoxy-2-(2-methoxyethoxy)ethane
DLS	dynamic light scattering
DMF	*N*,*N*-dimethylformamide
DMSO	dimethyl sulfoxide
DTA	differential thermal analysis
EDX	energy-dispersive X-ray spectroscopy
EELS	electron energy loss spectroscopy
EG	ethylene glycol
EPOP	ethylene diamine-based porous organic polymers
EPR	electron paramagnetic resonance
ESI-TOFMS	electrospray ionisation time-of-flight mass spectrometry
ESR	ethanol steam reforming
FC	field cooling
fcc	face-centred cubic
FFT	fast-Fourier transform
FE-SEM	field emission scanning electron microscopy
FMR	ferromagnetic resonance
FTIR	fourier-transform infrared spectroscopy
hcp	hexagonal close packed
HCS	hollow carbon spheres
HER	hydrogen evolution reaction
HRTEM	high-resolution transmission electron microscopy
ILs	ionic liquids
L-AA	L-ascorbic acid
MPs	microparticles
MWCNTs	multi-walled carbon nanotubes
N-CNFs	*N*-doped carbon nanofibres
Nd:YAG	neodymium-doped yttrium aluminium garnet
NMR	nuclear magnetic resonance
NPs	nanoparticles
OA	(9*Z*)-octadec-9-enoic acid
OAm	(*Z*)-octadec-9-enylamine
OER	oxygen evolution reaction
OMC	ordered mesoporous carbon
ORR	oxygen reduction reaction
PAA	poly(acrylic acid)
PS-*b*-PAA	polystyrene-*b*-poly(acrylic acid)
PS-*b*-PAA_{12}	polystyrene-*b*-poly(acrylic acid) with 12 mol% of poly(acrylic acid)
PS-*b*-PAA_8	polystyrene-*b*-poly(acrylic acid) with 8 mol% of poly(acrylic acid)
PVP	1-ethenylpyrrolidin-2-one
RGO	reduced graphene oxide
RF	resorcinol–formaldehyde
SAED	selected area electron diffraction
SAXS	small angle X-ray scattering
SEM	scanning electron microscopy
SERS	surface enhanced Raman spectroscopy
SQUID	superconducting quantum interference device
SWCNT	single-walled carbon nanotubes
TAP	tetraaminephthalocyanine
TEM	transmission electron microscopy
TGA	thermogravimetric analysis
TOP	trioctylphosphane
TOPO	trioctyl-λ^5-phosphanone
TPP	triphenylphosphane
UFPs	ultrafine particles
WAXS	wide angle X-ray scattering
XPS	X-ray photoelectron spectroscopy
XRD	X-ray diffraction analysis
ZFC	zero-field cooling
[BMI][NTf_2]	1-*n*-butyl-3-methylimidazolium *N*-bis (trifluoromethanesulfonyl) imidate
[DMI][BF_4]	1-*n*-decyl-3-methylimidazolium tetrafluoroborate
[DMI][FAP]	1-*n*-decyl-3-methylimidazolium trifluoro-tris(pentafluoroethane) phosphate
[DMI][NTf_2]	1-*n*-decyl-3-methylimidazolium *N*-bis-(trifluoromethanesulfonyl) imidate
[TDMI][NTf_2]	1-*n*-tetradecyl-3-methylimidazolium *N*-bis-(trifluoromethanesulfonyl) imidate

Acknowledgements

A. F. K. and D. G. Y. are thankful to the Government assignment for FRC Kazan Scientific Center of RAS for financial support of this research activity. The part of the work related to the analysis of the methods for preparation of cobalt nanoparticles was performed in the Arbuzov Institute of Organic and Physical Chemistry, FRC Kazan Scientific Center of RAS, and the testing of the catalytic activity has been done in Kazan Federal University. A. F. K. acknowledges support from the Erasmus + EU program (E + KA107) during her stay in Leipzig, Germany. M. C. acknowledges financial support from the Italian Ministry for University and Research (MIUR) for the project PRIN 2017 FERMAT "Fast electron dynamics in novel hybrid 2D materials". Open access funding enabled and organized by Projekt DEAL.

Conflict of Interest

The authors declare no conflict of interest.

© 2021 The Authors. European Journal of Inorganic Chemistry published by Wiley-VCH GmbH

Keywords: Cobalt · Electrochemistry · Nanoparticles · Physical and chemical methods · Synthesis design

[1] D. Astruc, *Chem. Rev.* **2020**, *120*, 461–463.
[2] G. Chen, I. Roy, C. Yang, P. N. Prasad, *Chem. Rev.* **2016**, *116*, 2826–2885.
[3] M. Pagliaro, *Chem. Eur. J.* **2015**, *21*, 11931–11936.
[4] G. Chen, J. Seo, C. Yang, P. N. Prasad, *Chem. Soc. Rev.* **2013**, *42*, 8304–8338.
[5] G. A. Ozin, *Adv. Mater.* **1992**, *4*, 612–651.
[6] https://en.wikipedia.org/wiki/Nanoparticle, **2021**.
[7] J. Zhang, J. Xu, Y. Wang, H. Xue, H. Pang, *Chem. Rec.* **2018**, *18*, 91–104.
[8] D. Wouters, U. S. Schubert, *Angew. Chem. Int. Ed.* **2004**, *43*, 2480–2495; *Angew. Chem.* **2004**, *116*, 2534–2550.
[9] L. Levy, Y. Sahoo, K.-S. Kim, E. J. Bergey, P. N. Prasad, *Chem. Mater.* **2002**, *14*, 3715–3721.
[10] G. M. Whitesides, J. P. Mathias, C. T. Seto, *Science* **1991**, *254*, 1312–1319.
[11] G. Chen, H. Qiu, P. N. Prasad, X. Chen, *Chem. Rev.* **2014**, *114*, 5161–5214.
[12] P. P. Edwards, J. M. Thomas, *Angew. Chem. Int. Ed.* **2007**, *46*, 5480–5486; *Angew. Chem.* **2007**, *119*, 5576–5582.
[13] L. Guczia, G. Peto, A. Becka, Z. Paszti, *Top. Catal.* **2004**, *29*, 129–130.
[14] N. Yan, Y. Yuan, P. J. Dyson, *Dalton Trans.* **2013**, *42*, 13294–13304.
[15] A.-H. Lu, E. L. Salabas, F. Schuth, *Angew. Chem. Int. Ed.* **2007**, *46*, 1222–1244; *Angew. Chem.* **2007**, *119*, 1242–1266.
[16] Y. Sun, S. Gao, F. Lei, C. Xiao, Y. Xie, *Acc. Chem. Res.* **2015**, *48*, 3–12.
[17] R. Feynman, *Eng. Sci.* **1960**, *23*, 22–36.
[18] F. Fu, Q. Wang, R. Ciganda, A. M. Martinez-Villacorta, A. Escobar, S. Moya, E. Fouquet, J. Ruiz, D. Astruc, *Chem. Eur. J.* **2018**, *24*, 6645–6653.
[19] X. Huang, X. Xiao, W. Zhang, X. Fan, L. Zhang, C. Cheng, S. Li, H. Ge, Q. Wang, L. Chen, *Phys. Chem. Chem. Phys.* **2017**, *19*, 4019–4029.
[20] A. Kleibert, J. Passig, K.-H. Meiwes-Broer, *J. Appl. Phys.* **2007**, *101*, 114318.
[21] R. Narayanan, M. A. El-Sayed, *J. Phys. Chem. B* **2005**, *109*, 12663–12676.
[22] C. N. R. Rao, G. U. Kulkarni, A. Govindaraj, B. C. Satishkumar, P. J. Thomas, *Pure Appl. Chem.* **2000**, *72*, 21–33.
[23] L. Prodi, *New J. Chem.* **2005**, *29*, 20–31.
[24] A. R. J. Azar, S. Mohebbi, *Mater. Chem. Phys.* **2015**, *168*, 85–94.
[25] R. Klajn, L. Fang, A. Coskun, M. A. Olson, P. J. Wesson, J. Fraser Stoddart, B. A. Grzybowski, *J. Am. Chem. Soc.* **2009**, *131*, 4233–4235.
[26] A. C. Balazs, T. Emrick, T. P. Russell, *Science* **2006**, *314*, 1107–1110.
[27] G. A. Ozin, L. Cademartiri, *Small* **2009**, *5*, 1240–1244.
[28] J. I. Martinez-Araya, G. Salgado-Moraan, D. Glossman-Mitnik, *J. Phys. Chem. B* **2013**, *117*, 6339–6351.
[29] A. L. Buchachenko, *Russ. J. Phys. Chem. A* **2009**, *83*, 1637–1642.
[30] G. Chen, C. Yang, P. N. Prasad, *Acc. Chem. Res.* **2013**, *46*, 1474–1486.
[31] C. N. R. Rao, G. U. Kulkarni, P. J. Thomasa, P. P. Edwards, *Chem. Soc. Rev.* **2000**, *29*, 27–35.
[32] Q. Hu, C. Tuck, R. Wildman, R. Hague in *Handbook of Nanoparticles, Vol. 2* (Ed.: M. Aliofkhazraei), Springer International Publishing, **2015**, pp. 1219–1278.
[33] Y. Bai, H. Zhang, Y. Feng, L. Fang, Y. Wang, *J. Mater. Chem. A* **2016**, *4*, 9072–9079.
[34] Y. Pan, Y. Chen, Y. Lin, P. Cui, K. Sun, Y. Liu, C. Liu, *J. Mater. Chem. A* **2016**, *4*, 14675–14686.
[35] W. Yang, Y. Huang, J. Fan, Y. Yu, C. Yang, H. Li, *Nanoscale* **2016**, *8*, 4898–04902.
[36] J. Park, E. Kang, S. U. Son, H. M. Park, M. K. Lee, J. Kim, K. W. Kim, H.-J. Noh, J.-H. Park, C. J. Bae, J.-G. Park, T. Hyeon, *Adv. Mater.* **2005**, *17*, 429–434.
[37] M. J. H. Ojea, A. P. Balague, D. R. Maneru, E. C. Sanudo, *J. Nanopart. Res.* **2014**, *16*, 2209–2217.
[38] M. Galaburda, V. Bogatyrov, O. Oranska, V. Gunko, J. Skubiszewska-Zieba, I. Urubkov, *J. Therm. Anal. Calorim.* **2015**, *122*, 553–561.
[39] P. Munnik, P. E. de Jongh, K. P. de Jong, *J. Am. Chem. Soc.* **2014**, *136*, 7333–7340.
[40] B. J. McNicholas, J. D. Blakemore, A. B. Chang, C. M. Bates, W. W. Kramer, R. H. Grubbs, H. B. Gray, *J. Am. Chem. Soc.* **2016**, *138*, 11160–11163.
[41] D. M. Clifford, C. E. Castano, J. V. Rojas, *Radiat. Phys. Chem.* **2017**, *132*, 52–64.
[42] A. Bai, C.-C. Hua, T.-C. Wen, *Electrochim. Acta* **2003**, *48*, 2425–2434.
[43] A. Bai, C.-C. Hu, *Electrochem. Commun.* **2003**, *5*, 78–82.
[44] I. Islam, S. A. Khandy, M. B. Zaman, D. C. Gupta, A. K. Hafiz, A. M. Siddiqui, *J. Mater. Sci. Mater. Electron.* **2018**, *29*, 3952–3956.
[45] N. Miguel-Sancho, G. Martinez, V. Sebastian, A. Malumbres, I. Florea, R. Arenal, M. C. Ortega-Liebana, J. L. Hueso, J. Santamaria, *ACS Appl. Mater. Interfaces* **2017**, *9*, 41529–41536.
[46] Y. Mahara, H. Ishikawa, J. Ohyama, K. Sawabe, A. Satsuma, *Catal. Today* **2016**, *265*, 2–6.
[47] A. P. Safronov, G. V. Kurlyandskaya, A. A. Chlenova, M. V. Kuznetsov, D. N. Bazhin, I. V. Beketov, M. B. Sanchez-Ilarduya, A. Martinez-Amesti, *Langmuir* **2014**, *30*, 3243–3253.
[48] T. M. Eggenhuisen, H. Friedrich, F. Nudelman, J. Zecevic, N. A. J. M. Sommerdijk, P. E. de Jongh, K. P. de Jong, *Chem. Mater.* **2013**, *25*, 890–896.
[49] X. Liu, J. Ruiz, D. Astruc, *J. Inorg. Organomet. Polym.* **2018**, *28*, 399–406.
[50] G. Peng, M. Mavrikakis, *Nano Lett.* **2015**, *15*, 629–634.
[51] J. D. Scholten, B. C. Leal, J. Dupont, *ACS Catal.* **2012**, *2*, 184–200.
[52] A. Gual, C. Godard, S. Castillon, C. Claver, *Dalton Trans.* **2010**, *39*, 11499–11512.
[53] Y. Kim, D. D. Torres, P. K. Jain, *Nano Lett.* **2016**, *16*, 3399–3407.
[54] C. T. Campbell, *Acc. Chem. Res.* **2013**, *46*, 1712–1719.
[55] L. Borchard, F. Hasche, M. R. Lohe, M. Oschatz, F. Schmidt, E. Kockrick, C. Ziegler, T. Lescouet, A. Bachmatiuk, B. Buchner, D. Farrusseng, P. Strasser, S. Kaskel, *Carbon* **2012**, *50*, 1861–1870.
[56] L. Yang, J. Kong, D. Zhou, J. M. Ang, S. L. Phua, W. A. Yee, H. Liu, Y. Huang, X. Lu, *Chem. Eur. J.* **2014**, *20*, 7776–7783.
[57] G. Guisbiers, G. Abudukelimu, D. Hourlier, *Nanoscale Res. Lett.* **2011**, *6*, 396–401.
[58] M. Yoon, Y. Kim, Y. M. Kim, H. Yoon, V. Volkov, A. Avilov, Y. J. Park, I.-W. Park, *J. Magn. Magn. Mater.* **2004**, *272–276*, 1259–1261.
[59] G. Vijayaprasath, R. Murugan, T. Mahalingam, G. Ravi, *J. Mater. Sci. Mater. Electron.* **2015**, *26*, 7205–7213.
[60] S. Kumar, S. Kumar, S. Jain, N. K. Verma, *Appl. Nanosci.* **2012**, *2*, 127–131.
[61] C. Pereira, A. M. Pereira, C. Fernandes, M. Rocha, R. Mendes, M. P. Fernandez-Garcia, A. Guedes, P. B. Tavares, J.-M. Greneche, J. P. Araujo, C. Freire, *Chem. Mater.* **2012**, *24*, 1496–1504.
[62] X.-M. Lin, A. C. S. Samia, *J. Magn. Magn. Mater.* **2006**, *305*, 100–109.
[63] B. Iss, I. M. Obaidat, B. A. Albiss, Y. Haik, *Int. J. Mol. Sci.* **2013**, *14*, 21266–21305.
[64] A. Akbarzadeh, M. Samiei, S. Davaran, *Nanoscale Res. Lett.* **2012**, *7*, 144.
[65] H. Hu, W. Zhang, *Opt. Mater.* **2006**, *28*, 536–550.
[66] M. A. Meyers, A. Mishra, D. J. Benson, *Prog. Mater. Sci.* **2006**, *51*, 427–556.
[67] D. Guo, G. Xie, J. Luo, *J. Phys. D* **2014**, *47*, 013001.
[68] M. C. C. Wobbe, M. A. Zwijnenburg, *Phys. Chem. Chem. Phys.* **2015**, *17*, 28892–28900.
[69] Y. Hu, C. Ji, X. Wang, J. Huo, Q. Liu, Y. Song, *Sci. Rep.* **2017**, *7*, 16485.
[70] G. Anandha babu, G. Ravi, *Appl. Phys. A* **2016**, *122*, 177.
[71] L. Arda, O. Ozturk, E. Asikuzun, S. Ataoglu, *Powder Technol.* **2013**, *235*, 479–484.
[72] S. Willing, H. Lehmann, M. Volkmann, C. Klinke, *Sci. Adv.* **2017**, *3*, 1603191.
[73] C. Quan, Z. Qin, Y. Zhu, Z. Wang, J. Zhang, W. Mao, X. Wang, J. Yang, X. Li, W. Huang, *J. Mater. Sci. Mater. Electron.* **2017**, *28*, 3278–3284.
[74] P. Parida, A. Kundu, S. K. Pati, *J. Cluster Sci.* **2009**, *20*, 355–364.
[75] S. S. Jawoor, S. A. Patil, M. Kumbar, P. B. Ramawadgi, *J. Mol. Struct.* **2018**, *1164*, 378–385.
[76] Y. Shin, I.-T. Bae, B. W. Arey, G. J. Exarhos, *Mater. Lett.* **2007**, *61*, 3215–3217.
[77] J. Wang, *Analyst* **2005**, *130*, 421–426.
[78] M. Auffan, J. Rose, J.-Y. Bottero, G. V. Lowry, J.-P. Jolivet, M. R. Wiesner, *Nat. Nanotechnol.* **2009**, *4*, 634–702.
[79] A. Azam, A. S. Ahmed, M. Oves, M. S. Khan, S. S. Habib, A. Memic, *Int. J. Nanomed.* **2012**, *7*, 6003–6009.
[80] J. D. Aiken III, R. G. Finke, *J. Mol. Catal. A* **1999**, *145*, 1–44.
[81] L. D. Pachon, G. Rothenberg, *Appl. Organomet. Chem.* **2008**, *22*, 288–299.
[82] V. Rahneshin, F. Khosravi, D. A. Ziolkowska, J. B. Jasinski, B. Panchapakesan, *Sci. Rep.* **2016**, *6*, 34831.
[83] W. J. Stark, P. R. Stoessel, W. Wohlleben, A. Hafner, *Chem. Soc. Rev.* **2015**, *44*, 5793–5805.
[84] M. Mazaheri, N. Eslahi, F. Ordikhani, E. Tamjid, A. Simchi, *Int. J. Nanomed.* **2015**, *10*, 6039–6054.

© 2021 The Authors. European Journal of Inorganic Chemistry published by Wiley-VCH GmbH

[85] S. Edebali, Y. Oztekin, G. Arslan in *Handbook of Nanomaterials for Industrial Applications, Chapter 4* (Ed.: C. M. Hussain), Elsevier, Amsterdam, **2018**, pp. 67–73.
[86] C.-C. You, A. Verma, V. M. Rotello, *Soft Matter* **2006**, *2*, 190–204.
[87] J. V. Barth, G. Costantini, K. Kern, *Nature* **2005**, *437*, 671–681.
[88] X. Liu, X. Wen, R. Hoffmann, *ACS Catal.* **2018**, *8*, 3365–3375.
[89] K.-R. Kim, J. Kang, K.-J. Chae, *Int. J. Hydrogen Energy* **2017**, *42*, 27623–27629.
[90] O. Marin-Flores, T. Turba, C. Ellefson, K. Wang, J. Breit, Jeongmin Ahnb, M. G. Norton, S. Ha, *Appl. Catal. B* **2010**, *98*, 186–192.
[91] S. P. Gubin, in *Magnetic Nanoparticles*, Wiley-VCH, Weinheim, **2009**, pp. 1–19.
[92] C. B. Murray, S. Sun, H. Doyle, T. Betley, *MRS Bull.* **2001**, *26*, 985–991.
[93] H. Tian, X. Li, L. Zeng, J. Gong, *ACS Catal.* **2015**, *5*, 4959–4977.
[94] J. Liang, M. Hassan, D. Zhu, L. Guo, X. Bo, *J. Colloid Interface Sci.* **2017**, *490*, 576–586.
[95] W. Zhang, H. Qi, L. Li, X. Wang, J. Chen, K. Peng, Z. Wang, *Green Chem.* **2009**, *11*, 1194–1200.
[96] L. M. Rossi, N. J. S. Costa, F. P. Silva, R. V. Gonsalves, *Nanotechnol. Rev.* **2013**, *2*, 597–614.
[97] W. B. Aziza, J. F. Petit, U. B. Demirci, Q. Xu, P. Miele, *Int. J. Hydrogen Energy* **2014**, *39*, 16919–16926.
[98] A. T. Montoya, E. G. Gillan, *ACS Omega* **2018**, *3*, 2947–2955.
[99] A. Kleibert, A. Balan, R. Yanes, P. M. Derlet, C. A. F. Vaz, M. Timm, A. F. Rodriguez, A. Beche, J. Verbeeck, R. S. Dhaka, M. Radovic, U. Nowak, F. Nolting, *Phys. Rev. B* **2017**, *95*, 195404.
[100] C. Binns, J. A. Blackman, in *Handbook of Metal Physics, Chapter 8*, Elsevier, Amsterdam, **2008**, pp. 231–277.
[101] E. M. M. Ibrahim, A. M. Abu-Dief, A. Elshafaie, A. M. Ahmed, *Mater. Chem. Phys.* **2017**, *192*, 41–47.
[102] D. Fan, J. Feng, S. Zhang, X. Lv, T. Gao, J. Xie, J. Liu, *J. Alloys Compd.* **2016**, *689*, 153–160.
[103] S. Mondini, A. Puglisi, M. Benaglia, D. Ramella, C. Drago, A. M. Ferretti, A. Ponti, *J. Nanopart. Res.* **2013**, *15*, 2025.
[104] G. Yu. Yurkov, D. A. Baranov, I. P. Dotsenko, S. P. Gubin, *Composites Part B* **2006**, *37*, 413–417.
[105] J. Bansmann, A. Kleibert, M. Getzlaff, A. F. Rodriguez, F. Nolting, C. Boeglin, K.-H. Meiwes-Broer, *Phys. Status Solidi B* **2010**, *247*, 1152–1160.
[106] C. Li, Q. Wu, M. Yue, H. Xu, S. Palaka, K. Elkins, J. P. Liu, *AIP Adv.* **2017**, *7*, 056229.
[107] M. Jercinovic, N. Radic, M. Buljan, J. Grenzer, I. Delac-Marion, M. Kralj, I. Bogdanovic-Radovic, R. Hubner, P. Dubcek, K. Salamon, S. Bernstorff, *J. Nanopart. Res.* **2014**, *16*, 2296–2306.
[108] Y.-M. Kim, K.-H. Kim, B. Kim, H. Choi, *J. Alloys Compd.* **2016**, *658*, 824–831.
[109] Y. Wang, Y. Zheng, S. Hu, *J. Phys. Chem. Solids* **2017**, *100*, 78–82.
[110] K.-C. Huang, K.-S. Chou, *Electrochem. Commun.* **2007**, *9*, 1907–1912.
[111] R. D. Murphy, M. J. Abere, K. J. Schrider, B. Torralva, S. M. Yalisove, *Appl. Phys. Lett.* **2013**, *103*, 093113.
[112] W. J. Tseng, C.-N. Chen, *J. Mater. Sci.* **2006**, *41*, 1213–1219.
[113] J. H. Mokkath, *J. Mater. Chem. C* **2018**, *6*, 2225–2228.
[114] I. Lukitsa, G. Nikolaychuk, O. Moroz, *Phys. Status Solidi C* **2014**, *11*, 1064–1067.
[115] Q. Xing, Z. Han, S. Zhao, *Mater. Lett.* **2017**, *188*, 103–106.
[116] G.-S. Lai, H.-L. Zhang, D.-Y. Han, *Anal. Lett.* **2008**, *41*, 3088–3099.
[117] A. S. Adekunle, K. I. Ozoemena, *Int. J. Electrochem. Sci.* **2010**, *5*, 1726–1742.
[118] F. E. Rasmussen, J. T. Ravnkilde, P. T. Tang, O. Hansen, S. Bouwstra, *Sens. Actuators A* **2001**, *9*, 242–248.
[119] G. I. Frolov, *Tech. Phys.* **2001**, *46*, 1537–1544.
[120] R. D. Shull, *IEEE Trans. Magn.* **1993**, *29*, 2614–2615.
[121] D. Ho, X. Sun, S. Sun, *Acc. Chem. Res.* **2011**, *44*, 875–882.
[122] A. Roucoux, K. Philippot, in *New Trends in the Design of Metal Nanoparticles and Derived Nanomaterials for Catalysis, Chapter 1*, Wiley-VCH, Weinheim, **2021**, pp. 1–11.
[123] C. Pohlmann, M. Sprinzl in *RNA and DNA Diagnostics* (Eds.: V. A. Erdmann, S. Jurga, J. Barciszewski), Springer International Publishing, **2015**, pp. 21–48.
[124] T. Yoon, J. Kim, J. Kim, J. K. Lee, *Energies* **2013**, *6*, 4830–4840.
[125] R. J. White, R. Luque, V. L. Budarin, J. H. Clark, D. J. Macquarrie, *Chem. Soc. Rev.* **2009**, *38*, 481–494.
[126] P. Mahamallik, A. Pal, *J. Environ. Chem. Eng.* **2017**, *5*, 2886–2893.
[127] N. Gad, M. R. Abdel-Moez, *Int. J. ChemTech Res.* **2015**, *8*, 85–92.
[128] K. Kajiwara, K. Sunaga, T. Tsuda, A. Sugaya, E. Sugaya, M. Kimura, *Biochem. Biophys. Res. Commun.* **2008**, *371*, 375–379.
[129] F. C. Campbell, in: *Elements of Metallurgy and Engineering Alloys, Chapter 20*, ASM International **2008**, pp. 371–394.
[130] M. Hawkins, *Appl. Earth Sci.* **2013**, *110*, 66–70.
[131] R. D. Armstrong, G. W. D. Briggs, E. A. Charles, *J. Appl. Electrochem.* **1988**, *18*, 215–219.
[132] E. White, E. Rinko, T. Prost, T. Horn, C. Ledford, C. Rock, I. Anderson, *Appl. Sci.* **2019**, *9*, 4843.
[133] S. S. Maroufian, P. Pillay, *IEEE Trans. Ind. Appl.* **2020**, *55*, 4733–4742.
[134] G. Qiao, M. Wang, F. Liu, Y. Liu, P. Zheng, Y. Sui, *IEEE Trans. Magn.* **2019**, *55*, 8664449.
[135] X. Han, J. Sun, T. Liu, H. Wang, Y. Zhang, C. Cui, *J. Alloys Compd.* **2019**, *785*, 715–724.
[136] C. Ropp, C. Chen, M. Greer, J. Glickstein, L. Mair, O. Hale, D. Ariando, S. Jafari, A. Hevaganinge, S. Mandal, I. N. Weinberg, *J. Magn. Reson.* **2019**, *303*, 82–90.
[137] J. Mohapatra, M. Xing, J. Elkins, J. P. Liu, *J. Alloys Compd.* **2020**, *824*, 153874.
[138] S. Sharma, B. Patil, A. Pathak, S. Ghosalkar, H. K. Mohanta, B. Roy, *Clean Technol. Environ. Policy* **2018**, *20*, 695–701.
[139] J. van de Loosdrecht, B. Balzhinimaev, J.-A. Dalmon, J. W. Niemantsverdriet, S. V. Tsybulya, A. M. Saib, P. J. van Berge, J. L. Visagie, *Catal. Today* **2007**, *123*, 293–302.
[140] C. Gosmini, J.-M. Begouin, A. Moncomble, *Chem. Commun.* **2008**, 3221–3233.
[141] T. Andou, Y. Saga, H. Komai, S. Matsunaga, M. Kanai, *Angew. Chem. Int. Ed.* **2013**, *52*, 3213–3216; *Angew. Chem.* **2013**, *125*, 3295–3298.
[142] M. Moselage, J. Li, L. Ackermann, *ACS Catal.* **2016**, *6*, 498–525.
[143] B. D. Ravetz, K. E. Ruhl, T. Rovis, *ACS Catal.* **2018**, *8*, 5323–5327.
[144] H. Wen, X. Wan, Z. Huang, *Angew. Chem. Int. Ed.* **2018**, *57*, 6319–6323; *Angew. Chem.* **2018**, *130*, 6427–6431.
[145] L. Wang, L. Wang, J. Zhang, X. Liu, H. Wang, W. Zhang, Q. Yang, J. Ma, X. Dong, S. J. Yoo, J.-G. Kim, X. Meng, F.-S. Xiao, *Angew. Chem. Int. Ed.* **2018**, *57*, 6104–6108; *Angew. Chem.* **2018**, *130*, 6212–6216.
[146] S. Roy, S. K. Das, B. Chattopadhyay, *Angew. Chem. Int. Ed.* **2018**, *57*, 2238–2243; *Angew. Chem.* **2018**, *130*, 2260–2265.
[147] Y. Kommagalla, K. Yamazaki, T. Yamaguchi, N. Chatani, *Chem. Commun.* **2018**, *54*, 1359–1362.
[148] T. T. Nguyen, L. Grigorjeva, O. Daugulis, *Angew. Chem. Int. Ed.* **2018**, *57*, 1688–1691; *Angew. Chem.* **2018**, *130*, 1704–1707.
[149] D. Xu, Q. Sun, Z. Quan, X. Wang, W. Sun, *Asian J. Org. Chem.* **2018**, *7*, 155–159.
[150] L. Zeng, H. Li, S. Tang, X. Gao, Y. Deng, G. Zhang, C.-W. Pao, J.-L. Chen, J.-F. Lee, A. Lei, *ACS Catal.* **2018**, *8*, 5448–5453.
[151] H. L. Sang, S. Yu, S. Ge, *Chem. Sci.* **2018**, *9*, 973–978.
[152] N. Sauermann, R. Mei, L. Ackermann, *Angew. Chem. Int. Ed.* **2018**, *57*, 5090–5094; *Angew. Chem.* **2018**, *130*, 5184–5188.
[153] W. Ma, G. Jacobs, V. R. R. Pendyala, D. E. Sparks, W. D. Shafer, G. A. Thomas, A. MacLennan, Y. Hu, B. H. Davis, *Catal. Today* **2018**, *299*, 28–36.
[154] D. M. Clifford, C. E. Castano, J. V. Rojasa, *Radiat. Phys. Chem.* **2017**, *132*, 52–64.
[155] A. F. Kempa, *Principles and Practice of Radiation Therapy, Chapter 25* (Eds.: C. M. Washington, D. Leaver), Elsevier, Amsterdam, **2016**, pp. 536–548.
[156] M. F. L'Annunziata, in *Radioactivity: Introduction and History, From the Quantum to Quarks*, Elsevier, Amsterdam, **2016**, pp. 46–66.
[157] L. Leyssens, B. Vinck, C. Van Der Straeten, F. Wuyts, L. Maes, *Toxicology* **2017**, *387*, 43–56.
[158] W. Parak, L. Manna, F.C Simmel, D. Cerion, P. Alivisatos in *Nanoparticles: from theory to application* (Ed.: G. Schmid), Wiley Interscience, New York, **2004**, pp. 4–49.
[159] R. C. Ashoori, *Nature* **1996**, *379*, 413–419.
[160] D. P. Dinega, M. G. Bawendi, *Angew. Chem. Int. Ed.* **1999**, *38*, 1788–1791; *Angew. Chem.* **1999**, *111*, 1906–1909.
[161] S. Ram, *Mater. Sci. Eng.* **2001**, *304–306*, 923–927.
[162] S. M. Ansari, R. D. Bohr, K. R. Pai, D. Sen, S. Mazumder, K. Ghosh, Y. D. Kolekar, C. V. Ramana, *Appl. Surf. Sci.* **2017**, *414*, 171–187.
[163] S. M. Ansari, R. D. Bhor, K. R. Pai, D. Sen, S. Mazumder, K. Ghosh, Y. D. Kolekar, C. V. Ramana, *Appl. Surf. Sci.* **2017**, *414*, 171–187.
[164] E. A. Lewis, A. D. Jewell, G. Kyriakou, E. C. H. Sykes, *Phys. Chem. Chem. Phys.* **2012**, *14*, 7215–7224.
[165] T. Hayashi, T. Ohno, S. Yatsuya, R. Uyeda, *Jpn. J. Appl. Phys.* **1977**, *16*, 705–717.
[166] S. Kajiwara, S. Ohno, K. Honma, M. Uda, *Philos. Mag. Lett.* **1987**, *55*, 215–219.

© 2021 The Authors. European Journal of Inorganic Chemistry published by Wiley-VCH GmbH

[167] F. Fievet, J. P. Lagier, B. Blin, *Solid State Ionics* **1989**, *32–33*, 198–205.
[168] L. Yiping, G. C. Hadjipanayis, C. M. Sorensen, K. J. Klabunde, *J. Appl. Phys.* **1990**, *67*, 4502–4504.
[169] G. N. Glavee, K. J. Klabunde, C. M. Sorensen, G. C. Hadjipanayis, *Inorg. Chem.* **1993**, *32*, 474–477.
[170] G. N. Glavee, K. J. Klabunde, C. M. Sorensen, G. C. Hadjipanayis, *Langmuir* **1993**, *8*, 162–169.
[171] J. P. Chen, C. M. Sorensen, K. J. Klabunde, G. C. Hadjipanayis, *J. Appl. Phys.* **1994**, *76*, 6316–6318.
[172] J. Tanori, N. Duxin, C. Petit, I. Lisiecki, P. Veillet, M. P. Pileni, *Colloid Polym. Sci.* **1995**, *273*, 886–892.
[173] J. A. Becker, R. Schäfer, R. Festag, W. Ruland, J. H. Wendorff, J. Pebler, S. A. Quaiser, W. Helbig, M. T. Reetz, *J. Chem. Phys.* **1995**, *103*, 2520–2527.
[174] J. Osuna, D. de Caro, C. Amiens, B. Chaudret, E. Snoeck, M. Respaud, J.-M. Broto, A. Fert, *J. Phys. Chem.* **1996**, *100*, 14571–14574.
[175] D. Meisel, *Curr. Opin. Colloid Interface Sci.* **1997**, *2*, 188–191.
[176] J. D. Aiken III, R. G. Finke, *J. Mol. Catal. A* **1999**, *145*, 1–44.
[177] L. D. Pachon, G. Rothenberg, *Appl. Organomet. Chem.* **2008**, *22*, 288–299.
[178] J.-L. Do, T. Friscic, *ACS Cent. Sci.* **2017**, *3*, 13–19.
[179] M. J. Rak, T. Friscic, A. Moores, *RSC Adv.* **2016**, *6*, 58365–58370.
[180] V. Chaudhary, Y. Zhang, H. Parmar, V. Sharma, X. Tau, R. V. Ramanujan, *ChemistryOpen* **2018**, *7*, 590–598.
[181] R. Abu-Much, A. Gedanken, *Chem. Eur. J.* **2008**, *14*, 10115–10122.
[182] E. V. Gurentsov, A. V. Eremin, E. Yu. Mikheeva, S. A. Musikhin, *High Temp.* **2016**, *54*, 902–904.
[183] S. M. Arakelyan, V. P. Veiko, S. V. Kutrovskaya, A. O. Kucherik, A. V. Osipov, T. A. Vartanyan, T. E. Itina, *J. Nanopart. Res.* **2016**, *18*, 155–167.
[184] S. E. F. Kleijn, S. C. S. Lai, M. T. M. Koper, P. R. Unwin, *Angew. Chem. Int. Ed.* **2014**, *53*, 3558–3586; *Angew. Chem.* **2014**, *126*, 3630–3660.
[185] J. Sniekers, K. Verguts, N. R. Brooks, S. Schaltin, T. H. Phan, T. M. T. Huynh, L. V. Meervelt, S. D. Feyter, J. W. Seo, J. Fransaer, K. Binnemans, *Chem. Eur. J.* **2016**, *22*, 1010–1020.
[186] S. Kapoor, H. G. Salunke, B. M. Pande, S. K. Kulshreshtha, J. P. Mittal, *Mater. Res. Bull.* **1998**, *33*, 1555–1562.
[187] P. Boyer, M. Meunier, *J. Phys. Chem. C* **2012**, *116*, 8014–8019.
[188] I. Robinson, M. Volk, L. D. Tung, G. Caruntu, N. Kay, N. TK Thanh, *J. Phys. Chem. C* **2009**, *113*, 9497–9501.
[189] J. Y. Yang, K. S. Yoon, W. J. Choi, Y. H. Do, J. H. Kim, C. O. Kim, J. P. Hong, *Curr. Appl. Phys.* **2007**, *7*, 147–150.
[190] P. Chiquet, M. Chambonneau, V. D. Marca, J. Postel-Pellerin, P. Canet, S. Souiki-Figuigui, G. Idda, J.-M. Portal, D. Grojo, *Sci. Rep.* **2019**, *9*, 7392.
[191] M. Wuttig, H. Bhaskaran, T. Taubner, *Nature Photon.* **2017**, *11*, 465–476.
[192] A. S. Kashin, V. P. Ananikov, *Russ. Chem. Bull.* **2011**, *60*, 2602–2607.
[193] B.-X. Chung, C.-P. Liu, *Mater. Lett.* **2004**, *58*, 1437–1440.
[194] R. Sergiienko, E. Shibata, A. Zentaro, D. Shindo, T. Nakamura, G. Qin, *Acta Mater.* **2007**, *55*, 3671–3680.
[195] H. Liu, Y. Li, M. Yuan, G. Sun, H. Li, S. Ma, Q. Liao, Y. Zhang, *ACS Appl. Mater. Interfaces* **2018**, *10*, 22591–22601.
[196] J. S. Yin, Z. L. Wang, *Nanostruct. Mater.* **1999**, *11*, 845–852.
[197] C. Johans, M. Pohjakallio, M. Ijas, Y. Geb, K. Kontturi, *Colloids Surf. A* **2008**, *330*, 14–20.
[198] V. F. Puntes, K. M. Krishnan, P. Alivisatos, *Appl. Phys. Lett.* **2001**, *78*, 2187.
[199] V. F. Puntes, K. M. Krishnan, A. P. Alivisatos, *Science* **2001**, *291*, 2115–2117.
[200] V. F. Puntes, K. M. Krishnan, A. P. Alivisatos, *Top. Catal.* **2002**, *19*, 145–150.
[201] H. T. Yang, Y. K. Su, C. M. Shen, T. Z. Yang, H. J. Gao, *Surf. Interface Anal.* **2004**, *36*, 155–160.
[202] L. Wu, Q. Li, C. H. Wu, H. Zhu, A. Mendoza-Garcia, B. Shen, J. Guo, S. Sun, *J. Am. Chem. Soc.* **2015**, *137*, 7071–7074.
[203] H. G. Sanchez Casalongue, M. L. Ng, S. Kaya, D. Friebel, H. Ogasawara, A. Nilsson, *Angew. Chem. Int. Ed.* **2014**, *53*, 7169–7172; *Angew. Chem.* **2014**, *126*, 7297–7300.
[204] S. Anantharaj, S. Kundu, *ACS Energy Lett.* **2019**, *4*, 1260–1264.
[205] M. Scariot, D. O. Silva, J. D. Scholten, G. Machado, S. R. Teixeira, M. A. Novak, G. Ebeling, J. Dupont, *Angew. Chem. Int. Ed.* **2008**, *47*, 9075–9078; *Angew. Chem.* **2008**, *120*, 9215–9218.
[206] D. O. Silva, J. D. Scholten, M. A. Gelesky, S. R. Teixeira, A. C. B. D. Santos, E. F. Souza-Aguiar, J. Dupont, *ChemSusChem* **2008**, *1*, 291–294.
[207] V. Iablokov, S. K. Beaumont, S. Alayoglu, V. V. Pushkarev, C. Specht, J. Gao, A. P. Alivisatos, N. Kruse, G. A. Somorjai, *Nano Lett.* **2012**, *12*, 3091–3096.
[208] B. Morcos, P. Lecante, R. Morel, P.-H. Haumesser, C. C. Santini, *Langmuir* **2018**, *34*, 7086–7095.
[209] Q. Yang, Z. Zhang, X.-G. Sun, Y.-S. Hu, H. Xing, S. Dai, *Chem. Soc. Rev.* **2018**, *47*, 2020–2064.
[210] J. C. Park, J. I. Kwon, S. W. Kang, D. H. Chun, H.-T. Lee, H. Junga, J.-I. Yang, *RSC Adv.* **2017**, *7*, 8852–8857.
[211] H. Shao, Y. Huang, H. Lee, Y. J. Suh, C. O. Kim, *J. Magn. Magn. Mater.* **2006**, *304*, 28–30.
[212] B. D. Cullity in *Elements of X-ray Diffraction, Second Edition, Chapter 6* (Ed.: M. Cohen), Addison-Wesley Publishing Company, **1978**, pp. 161–185.
[213] X. Cui, K. Liang, M. Tian, Y. Zhu, J. Ma, Z. Dong, *J. Colloid Interface Sci.* **2017**, *501*, 231–240.
[214] J. Song, Z.-F. Huang, L. Pan, K. Li, X. Zhang, L. Wang, J.-J. Zou, *Appl. Catal. B* **2018**, *227*, 386–408.
[215] C. Z. Loebick, M. Majewska, F. Ren, G. L. Haller, L. D. Pfefferle, *J. Phys. Chem. C* **2010**, *114*, 11092–11097.
[216] P. Mente, T. N. Phaahlamohlaka, V. Mashindi, N. J. Coville, *J. Mater. Sci.* **2021**, *56*, 2113–2128.
[217] S. Liang, C. Liang, *Materials* **2019**, *12*, 243–259.
[218] S. Gopi, K. Giribabu, M. Kathiresan, K. Yun, *Sustain. Energy Fuels* **2020**, *4*, 3797–3805.
[219] J. Lia, Q. Wub, J. Wu in *Handbook of Nanoparticles, Vol. 2* (Ed.: M. Aliofkhazraei), Springer International Publishing, **2015**, pp. 295–328.
[220] J. Liu, Z. Wang, X. Yan, P. Jian, *J. Colloid Interface Sci.* **2017**, *505*, 789–795.
[221] N. C. Shin, Y.-H. Lee, Y. H. Shin, J. Kim, Y.-W. Lee, *Mater. Chem. Phys.* **2010**, *124*, 140–144.
[222] G. Seong, T. Adschiri, *Dalton Trans.* **2014**, *43*, 10778–10786.
[223] N. Singh, J. R. Ansari, M. Pal, N. T. K. Thanh, T. Le, A. Datta, *J. Mater. Sci. Mater. Electron.* **2020**, *31*, 15108–15117.
[224] C. M. Phan, H. M. Nguyen, *J. Phys. Chem. A* **2017**, *121*, 3213–3219.
[225] R. Javed, M. Zia, S. Naz, S. O. Aisida, N. Ain, Q. Ao, *J. Nanobiotechnol.* **2020**, *18*, 172–187.
[226] S. Campisi, M. Schiavoni, C. E. Chan-Thaw, A. Villa *Catalysts* **2016**, *6*, 185–206.
[227] S. Sun, C. B. Murray, *J. Appl. Phys.* **1999**, *85*, 4325–4330.
[228] F. X. Redl, K.-S. Cho, C. B. Murray, S. O'Brien, *Nature* **2003**, *423*, 968–971.
[229] Z. Zhang, X. Chen, X. Zhang, C. Shi, *Solid State Commun.* **2006**, *139*, 403–405.
[230] N. Wu, L. Fu, M. Su, M. Aslam, K. C. Wong, V. P. Dravid, *Nano Lett.* **2004**, *4*, 383–386.
[231] L. Meziane, C. Salzemann, C. Aubert, H. Gérard, C. Petit, M. Petit, *Nanoscale* **2016**, *8*, 18640–18645.
[232] A. Vivien, M. Guillaumont, L. Meziane, C. Salzemann, C. Aubert, S. Halbert, H. Gérard, M. Petit, C. Petit, *Chem. Mater.* **2019**, *31*, 960–968.
[233] P. Alex, S. Majumdar, J. Kishor, I. G. Sharma, *Mater. Sci. Appl.* **2011**, *02*, 1307–1312.
[234] S. A. Salman, T. Usami, K. Kuroda, M. Okido, *J. Nanobiotechnol.* **2014**, *2014*, 525193.
[235] F. Guo, H. Zheng, Z. Yang, Y. Qian, *Mater. Lett.* **2002**, *56*, 906–909.
[236] T. Kamal, S. B. Khan, S. Haider, Y. G. Alghamdi, A. M. Asiri, *Int. J. Biol. Macromol.* **2017**, *104*, 56–62.
[237] S. Chairam, P. Jarujamrus, M. Amatatongchai, *Adv. Nat. Sci. Nanosci. Nanotechnol.* **2019**, *10*, 025013.
[238] M. Imadadulla, M. Nemakal, L. K. Sannegowda, *New J. Chem.* **2018**, *42*, 11364–11372.
[239] C. Petit, A. Tale, M. P. Pileni, *J. Phys. Chem. B* **1999**, *103*, 1805–1810.
[240] C. Petit, M. P. Pileni, *Appl. Surf. Sci.* **2000**, *162–163*, 519–528.
[241] I. Lisiecki, M. P. Pileni, *Langmuir* **2003**, *19*, 9486–9489.
[242] Y.-W. Zhao, R. K. Zheng, X. X. Zhang, J. Q. Xiao, *IEEE Trans. Magn.* **2003**, *39*, 2764–2766.
[243] F. M. Abel, V. Tzitzios, G. C. Hadjipanayis, *J. Magn. Magn. Mater.* **2016**, *400*, 286–289.
[244] P. Riani, G. Garbarino, F. Canepa, G. Busca, *J. Chem. Technol. Biotechnol.* **2019**, *94*, 538–546.
[245] N. Bion, D. Duprez, F. Epron, *ChemSusChem* **2012**, *5*, 76–84.
[246] G. Garbarino, P. Riani, M. A. Lucchini, F. Canepa, S. Kawale, G. Busca, *Int. J. Hydrogen Energy* **2013**, *38*, 82–91.
[247] H. Mahdavi, M. Sajedi, T. Shahalizade, A. A. Heidari, *Polym. Bull.* **2020**, *77*, 4489–4505.
[248] A. S. Zola, R. U. Ribeiro, J. M. C. Bueno, D. Zanchet, P. A. Arroyo, *J. Exp. Nanosci.* **2014**, *9*, 398–405.

© 2021 The Authors. European Journal of Inorganic Chemistry published by Wiley-VCH GmbH

[249] F. Fievet, S. Ammar-Merah, R. Brayner, F. Chau, M. Giraud, F. Mammeri, J. Peron, J.-Y. Piquemal, L. Sicard, G. Viau, *Chem. Soc. Rev.* **2018**, *47*, 5187–5233.
[250] H. Dong, Y.-C. Chen, C. Feldmann, *Green Chem.* **2015**, *17*, 4107–4132.
[251] K. A. Atmane, C. Michel, J.-Y. Piquemal, P. Sautet, P. Beaunier, M. Giraud, M. Sicard, S. Nowak, R. Losno, G. Viau, *Nanoscale* **2014**, *6*, 2682–2692.
[252] H. Kaneko, T. Matsumoto, J. L. C. Huaman, M. Ishijima, K. Suzuki, H. Miyamura, J. Balachandran, *Inorg. Chem.* **2021**, *60*, 3025–3036.
[253] M. D. L. Balela, Z. Lockman, A. Azizan, E. Matsubara, A. V. Amorsolo Jr., *J. Phys. Sci.* **2008**, *19*, 1–11.
[254] R. J. Joseyphus, T. Matsumoto, H. Takahashi, D. Kodama, K. Tohji, B. Jeyadevan, *J. Solid State Chem.* **2007**, *180*, 3008–3018.
[255] K. Takahashi, S. Yokoyama, T. Matsumoto, J. L. C. Huaman, H. Kaneko, J.-Y. Piquemal, H. Miyamura, J. Balachandran, *New J. Chem.* **2016**, *40*, 8632–8642.
[256] W.-T. Cheng, H. W. Cheng, *AIChE J.* **2009**, *55*, 1383–1389.
[257] S. S. K. Kamal, P. K. Sahoo, M. Premkumar, N. V. R. Rao, T. J. Kumar, B. Sreedhar, A. K. Singh, S. Ram, K. C. Sekhar, *J. Alloys Compd.* **2009**, *474*, 214–218.
[258] N. Chakroune, G. Viau, C. Ricolleau, F. Fiévet-Vincent, F. Fiévet, *J. Mater. Chem.* **2003**, *13*, 312–318.
[259] Yu. Demidova, I. Simakova, I. Prosvirin, *Int. J. Nanotechnol.* **2016**, *13*, 3–14.
[260] K. Mrad, F. Schoenstein, H. T. T. Nong, E. Anagnostopoulou, A. Viola, L. Mouton, S. Mercone, C. Ricolleau, N. Jouini, M. Abderraba, L.-M. Lacroix, G. Viau, J.-Y. Piquemal, *CrystEngComm* **2017**, *19*, 3476–3484.
[261] M. Hytch, R. Arenal, L. Sicard, M. Giraud, J.-Y. Piquemal, G. Viau, *Nano Lett.* **2019**, *19*, 9160–9169.
[262] M. G. Montiel, P. Santiago-Jacinto, J. A. I. D. Gongora, E. Reguera, G. Rodriguez-Gattorno, *Nano-Micro Lett.* **2011**, *3*, 12–19.
[263] M. T. Reetz, W. Helbig, *J. Am. Chem. Soc.* **1994**, *116*, 7401–7402.
[264] D. G. Yakhvarov, A. F. Khusnuriyalova, O. G. Sinyashin, *Organometallics* **2014**, *33*, 4574–4589.
[265] S. M. Oja, Y. Fan, C. M. Armstrong, P. Defnet, B. Zhang, *Anal. Chem.* **2016**, *88*, 414–430.
[266] G. Saito, T. Akiyama, *J. Nanomater.* **2015**, *2015*, 1–21.
[267] I. Valov, W. D. Lu, *Nanoscale* **2016**, *8*, 13828–13837.
[268] X. Chia, A. Y. S. Eng, A. Ambrosi, S. M. Tan, M. Pumera, *Chem. Rev.* **2015**, *115*, 11941–11966.
[269] I. Gonzalez, D. Martinez, G. Jorge, C. Rojas, C. Urbina, *Microsc. Microanal.* **2004**, *10*, 494–495.
[270] A. Ledo-Suarez, L. Rodriguez-Sanchez, M. C. Blanco, M. A. Lopez-Quintela, *Phys. Status Solidi A* **2006**, *203*, 1234–1240.
[271] P. G. Schiavi, P. Altimari, F. Pagnanelli, E. Moscardini, L. Toro, *Chem. Eng.Trans.* **2015**, *43*, 673–678.
[272] P. G. Schiavi, P. Altimari, R. Zanoni, F. Pagnanelli, *Electrochim. Acta* **2016**, *220*, 405–416.
[273] P. G. Schiavi, P. Altimari, A. Rubino, F. Pagnanelli, *Electrochim. Acta* **2018**, *259*, 711–722.
[274] P. G. Schiavi, A. Rubino, P. Altimari, F. Pagnanelli, *AIP Conf. Proc.* **2018**, *1990*, 020005.
[275] V. V. Yanilkin, G. R. Nasretdinova, Y. N. Osin, V. V. Salnikov, *Electrochim. Acta* **2015**, *168*, 82–88.
[276] A. F. Khusnuriyalova, A. Petr, A. T. Gubaidullin, A. V. Sukhov, V. I. Morozov, B. Buchner, V. Kataev, O. G. Sinyashin, D. G. Yakhvarov, *Electrochim. Acta* **2018**, *260*, 324–329.

Manuscript received: April 30, 2021
Revised manuscript received: June 9, 2021
Accepted manuscript online: June 15, 2021

© 2021 The Authors. European Journal of Inorganic Chemistry published by Wiley-VCH GmbH